JACS
JOURNAL OF THE AMERICAN CHEMICAL SOCIETY
pubs.acs.org/JACS
Perspective

Controlling Nucleation Pathways in Zeolite Crystallization: Seeding Conceptual Methodologies for Advanced Materials Design

Rishabh Jain, Adam J. Mallette, and Jeffrey D. Rimer*

Cite This: J. Am. Chem. Soc. 2021, 143, 21446−21460
Read Online
ACCESS | Metrics & More | Article Recommendations

ABSTRACT: A core objective of synthesizing zeolites for widespread applications is to produce materials with properties and corresponding performances that exceed conventional counterparts. This places an impetus on elucidating and controlling processes of crystallization where one of the most critical design criteria is the ability to prepare zeolite crystals with ultrasmall dimensions to mitigate the deleterious effects of mass transport limitations. At the most fundamental level, this requires a comprehensive understanding of nucleation to address this ubiquitous materials gap. This Perspective highlights recent methodologies to alter zeolite nucleation by using seed-assisted protocols and the exploitation of interzeolite transformations to design advanced materials. Introduction of crystalline seeds in complex growth media used to synthesize zeolites can have wide-ranging effects on the physicochemical properties of the final product. Here we discuss the diverse pathways of zeolite nucleation, recent breakthroughs in seed-assisted syntheses of nanosized and hierarchical materials, and shortcomings for developing generalized guidelines to predict synthesis outcomes. We offer a critical analysis of state-of-the-art approaches to tailor zeolite crystallization wherein we conceptualize whether parallels between network theory and zeolite synthesis can be instrumental for translating key findings of individual discoveries across a broader set of zeolite crystal structures and/or synthesis conditions.

1. INTRODUCTION

The past 20 years has witnessed a resurgence in zeolite research owing to their role as catalysts in reactions such as emissions control,[1,2] C1 chemistry,[3] biomass conversion,[4,5] and most recently polymer recycling,[6,7] which has expanded their utility beyond traditional applications as sorbents in ion exchange and separations and as catalysts in the (petro)-chemical industry.[8,9] In the coming decades, it is paramount that innovations in zeolite design meet the demands of a shifting energy economy. There are several approaches that can be taken to address these changes. One option is new materials discovery; however, the most expedient is the optimization of known structures toward achieving exceptional physicochemical properties. This objective is nontrivial owing to the complex growth media and multiple mechanisms involved in zeolite crystallization, many of which are not well understood, thereby complicating efforts to develop causal relationships between synthesis parameters and crystal properties. With each new breakthrough in zeolite synthesis the key findings are seemingly constrained to few zeolite crystal structures under limited synthesis conditions. This prompts an open question: can translational research link findings among a broader set of materials in a more predictive manner? Achieving this level of design for advanced zeolitic materials relies on knowledge of nucleation and growth pathways to inform new synthesis strategies.

For decades, classical nucleation theory (CNT)[10,11] has been used to describe the birth of crystals based on the difference between surface and volumetric free energies of crystal formation (Figure 1A). In CNT, the energetic barrier for nucleation is correlated to a critical radius or size where there is equal probability for continued growth or dissolution. Models of nucleation and growth are governed by supersaturation where variations in solute concentration lead to predictable changes in nucleation rates and concomitant effects on crystal growth.[12] It has been reported, however, that CNT is unable to describe nucleation rates in many complex systems, such as proteins, colloids, biominerals, and zeolites.[13] This is particularly true for systems involving two-step nucleation,[14] which is a nonclassical pathway. According to this mechanism, liquid or solid-like clusters first densify to form a metastable phase. As crystallization progresses, clusters can undergo structural ordering with a free energy barrier for nucleation that is putatively less than that of the classical pathway (Figure 1A). A major difference between classical and two-step mechanisms is that solute densification and ordering occur simultaneously in the former but sequentially for the nonclassical pathway. When nucleation deviates from CNT, it is more challenging to predict how changes in the crystal growth medium will affect the properties of the final crystalline product and the mechanisms by which they are attained.

The sol gel medium in zeolite syntheses is composed of amorphous solids (or gels) in contact with solution.[19] Water is the most common solvent in zeolite synthesis, although prior

Received: October 18, 2021
Published: December 16, 2021

https://doi.org/10.1021/jacs.1c11014
J. Am. Chem. Soc. 2021, 143, 21446−21460

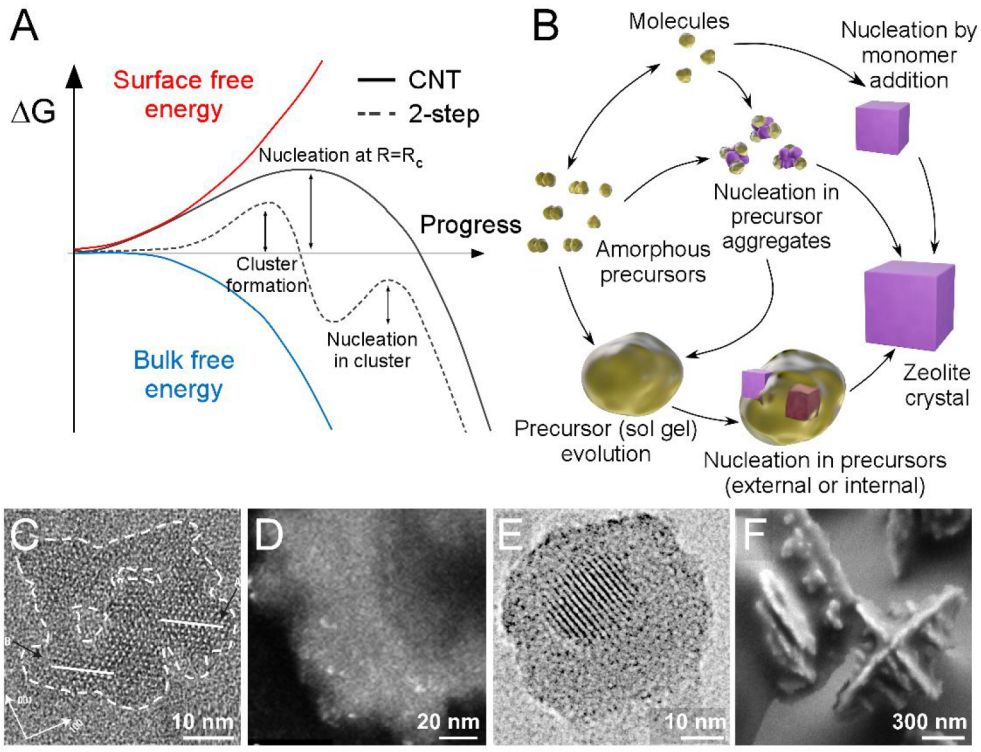

Figure 1. (A) General energetic landscape as a function of nucleation progress. Classical nucleation involves a single barrier that is overcome when fluctuations in local density lead to nucleus formation where those of critical radius (R_c) can grow or dissolve with equal probability. A two-step (or nonclassical) pathway involves the initial formation of clusters that lowers the barrier for nucleation. (B) Illustration of potential pathways for zeolite nucleation. (C−E) TEM images for three different zeolites: (C) Silicalite-1 (MFI) nucleus from the aggregation of amorphous precursors.[15] Reproduced with permission from ref 15. Copyright 2006 Springer Nature. (D) FAU nuclei (bright spots) on the surfaces of amorphous precursors.[16] Reproduced with permission from ref 16. (E) LTA nucleating within the interior of a gel particle. Reproduced from ref 17. Copyright 1999 AAAS. (F) SEM image of self-pillared pentasil nucleation on the surface of an amorphous precursor. Reproduced with permission from ref 18. Copyright 2021 John Wiley and Sons.

studies have explored alternative options (e.g., organics and ionic liquids).[20−24] Even in dry gel conversions (DGC), or so-called "solvent-free" syntheses,[25−28] water is present from the exchange between dry gel and the atmosphere as well as water generation from (alumino)silicate condensation. Nucleation can occur via a classical pathway from soluble species (molecules); however, most evidence points to nucleation by a two-step mechanism involving amorphous precursors. The diversity of precursors and their dynamic changes in physicochemical properties during the induction period can result in various zeolite nucleation mechanisms (Figure 1B). Tsapatsis and co-workers[15,29] have shown that silicalite-1 nucleation occurs within aggregates (ca. 50 nm) of amorphous precursors (2−6 nm) that densify and undergo disorder-to-order transitions to produce nuclei with shapes that are commensurate with the fractal geometry of the original aggregate (Figure 1C). Each region of the silicalite-1 nucleus, which corresponds to an original precursor, is predominantly in crystallographic registry with neighboring regions, while voids in the original aggregate are initially retained (Figure 1C, dashed circles). Nucleation can alternatively occur within agglomerates of amorphous precursors, which range from gels to worm-like particles.[17,19,30−35] Prior studies have shown that nucleation occurs on exterior surfaces of evolved amorphous phases for self-pillared pentasils (Figure 1F)[18] and faujasite (Figure 1D)[16] as well as gel surfaces for the latter.[31] In studies of zeolite A (Figure 1E)[17] it has been shown that nucleation occurs within the interior of gel-like particles. In studies where similar findings are reported, it is posited that nucleation occurs within gel cavities where a liquid phase is present.[36−38] However, the role of the solution phase in nucleation, particularly at the solid/liquid interface, is not well understood, nor are the factors controlling which pathway is dominant.

Probing nucleation events at the atomic level on relevant time scales is challenging. The difficulty of characterizing amorphous precursors is attributed in part to synthesis conditions producing large variations in precursor density, composition, hydration, and the occlusion of structure-directing agents (SDAs). These factors contribute to the ambiguous definition of "amorphous" for the precursors involved in nonclassical pathways, which is further complicated by their structural evolution with synthesis time,[39] suggesting a degree of local ordering that potentially facilitates heterogeneous nucleation. Several studies have identified strategies for controlling nucleation by altering the nature of precursors; for example, Larlus and Valtchev demonstrated that judicious selection of potassium concentration in LTL growth solutions can reduce precursor aggregation, thus leading to smaller crystals.[40] An alternative approach to promote nucleation is the introduction of crystalline seeds, which is a focal point of this Perspective. Seed-assisted synthesis (SAS) involves crystals of one zeolite framework being added to a growth mixture to produce a crystalline product with either the same or different framework. Other porous crystalline systems such as covalent organic frameworks (COFs) and metal−organic frameworks (MOFs) have utilized SAS strategies.[41−43] Among the many

https://doi.org/10.1021/jacs.1c11014
J. Am. Chem. Soc. 2021, 143, 21446−21460

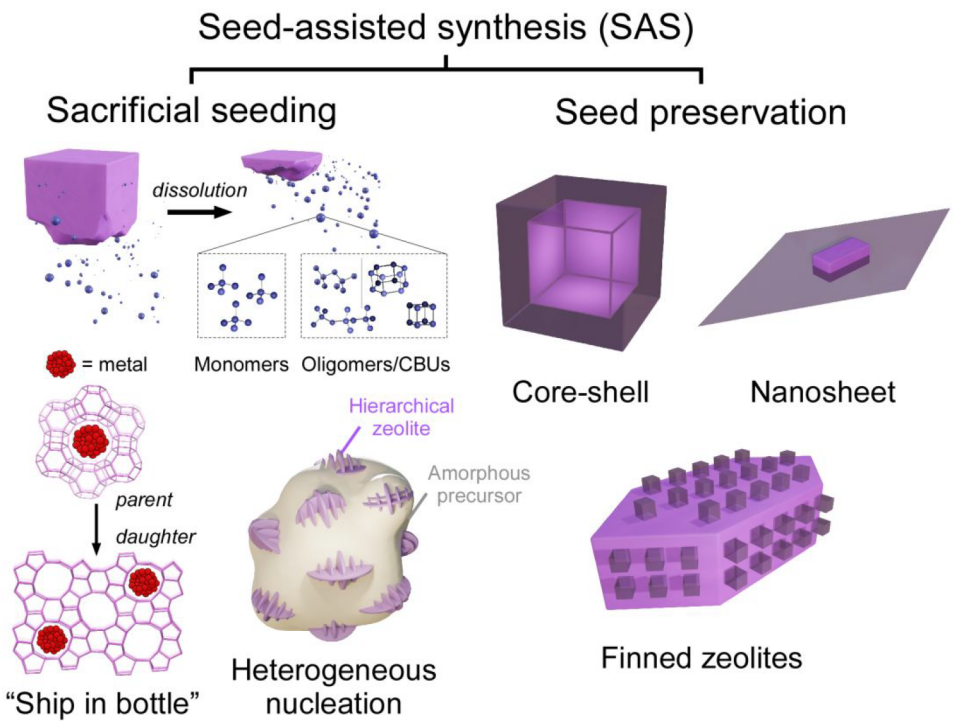

Figure 2. Seed-assisted synthesis can be categorized as processes where seeds are either sacrificed (left) or preserved (right). Seed dissolution can produce monomers and oligomers that alter supersaturation or may result in structured species (e.g., CBUs, rings) that retain some "memory" of the original seed. Examples of sacrificial seeding include metal encapsulation from interzeolite transformation[74,75] or hierarchical zeolites (e.g., self-pillared pentasils).[18] Examples of seed preservation include syntheses of core−shells (e.g., ZSM-5@silicalite-1),[80] nanosheets with rotational intergrowths,[81] and finned zeolites.[44]

benefits of SAS include access to zeolite properties that would otherwise be unattainable without seeds. In recent years there has been increased interest in SAS wherein seeds can be used as alternative (alumino)silicate sources, as solids for heterogeneous nucleation, or substrates for epitaxial growth.[44,45] SAS can be used to accelerate crystallization in either conventional batch processes[46−48] or continuous flow reactors.[49−51] The presence of seeds can improve the efficiency of zeolite syntheses by eliminating crystal impurities[52] or bypassing the need for organic structure-directing agents (OSDAs).[53,54] A common phenomenon in both SAS and nonseeded OSDA-free syntheses is interzeolite transformation (IZT)—a process involving the transformation of an initial thermodynamically metastable framework (seed or parent) into a different framework (product or daughter). Multiple IZT sequences can occur in any given synthesis where each stage results in a product that is more thermodynamically stable than the previous, seemingly in accordance with the Ostwald rule of stages.[55]

There have been several review articles written on topics of SAS, IZT, and zeolite synthesis that provide in-depth descriptions of synthesis techniques, material properties, and zeolite performance in different applications.[56−63] In this Perspective, we provide a conceptual overview of SAS pathways and highlight recent breakthroughs in the use of seeds to achieve novel materials—notably nanosized and hierarchical zeolites. Within the context of seed-assisted methods, we provide a synopsis of IZT and propose ways to explain (or potentially predict) trends in nucleation under different synthesis conditions. The impact of SAS and IZT on zeolite crystal size is discussed along with general guidelines for rationalizing parent−daughter relationships. We end with an overview of machine learning and data analytics as recent approaches to establish networks that link zeolite structures and synthesis conditions. On the basis of these models, we speculate whether network theory can be more generally applied in zeolite synthesis to connect the effects observed for one zeolite to others with disparate crystal structures.

2. SEED-ASSISTED SYNTHESIS

There are two classes of seed-assisted synthesis (SAS) differentiated by the fate of the original seeds (Figure 2). Sacrificial SAS involves seed dissolution and typically occurs when seeds are introduced at a low quantity relative to the total concentration of silica and alumina. The nature of dissolved species is unknown but could be monomers or (alumino)silicate oligomers or potentially composite building units (CBUs) and/or rings that retain some "memory" of the parent seed. Although studies have suggested that memory of the seed persists throughout dissolution and nucleation of the daughter zeolite,[64−69] it has been demonstrated that dissolved species may be oligomers lacking a high degree of local order.[56,70,71] The dissolved species can alter nucleation in ways that are not completely understood, such as promoting the emergence of nanosheets on the surfaces of amorphous precursors (Figure 2) that develop into self-pillared pentasils (SPPs).[18] When the seed (parent) and final product (daughter) are two different zeolite structures, this is termed an interzeolite transformation (IZT), which is discussed in section 3. IZT can be utilized in SAS to tailor zeolite properties (e.g., crystal size and shape)[72,73] or introduce metals into zeolite pores (Figure 2) that would otherwise be challenging to accomplish by conventional one-pot syntheses or postsynthesis

https://doi.org/10.1021/jacs.1c11014
J. Am. Chem. Soc. 2021, 143, 21446−21460

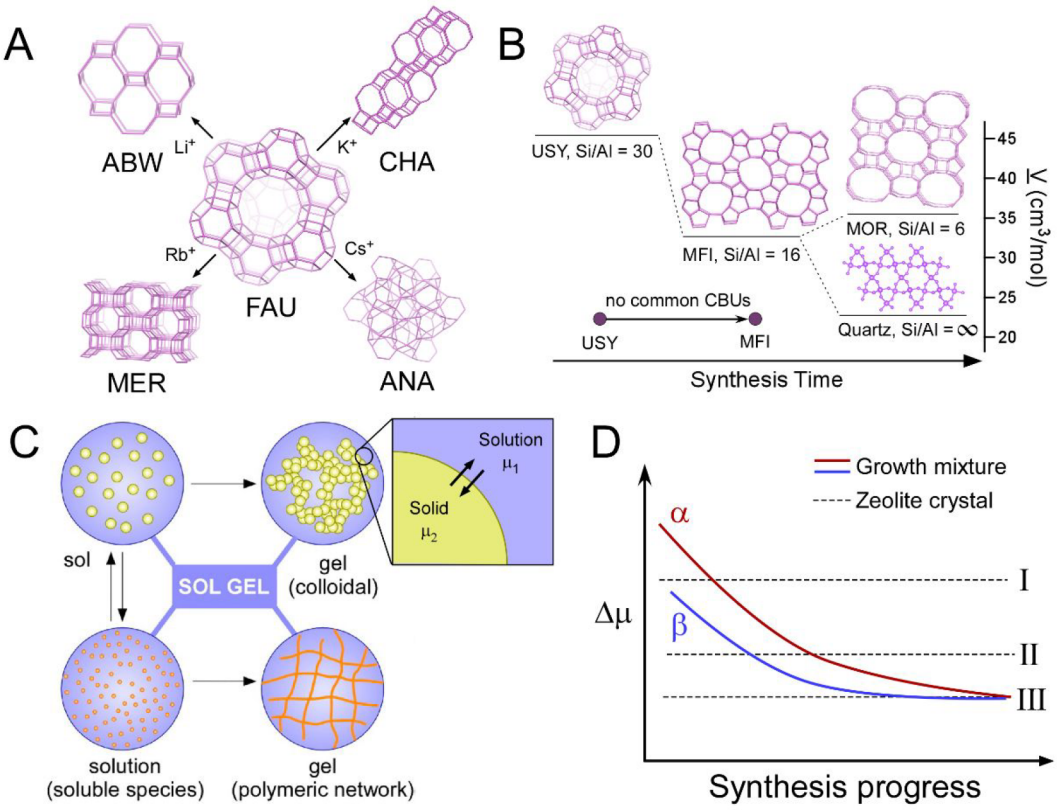

Figure 3. (A) Transformation of FAU (parent seed) into four distinct daughter zeolites in the presence of different alkali metal cations that function as inorganic SDAs. Reproduced with permission from ref 89. Copyright 2013 Royal Society of Chemistry. (B) Sequence of interzeolite transformation with increasing synthesis time where USY (FAU) seeds are used as the sole source of reagents in an organic-free growth mixture. The intermediate daughter, ZSM-5 (MFI), does not share a common CBU with the parent. The second IZT sequence leads to a mixture of mordenite (MOR) and quartz impurity. Reproduced with permission from ref 112. Copyright 2019 John Wiley and Sons. (C) Diverse physical states of the sol gel containing dispersed colloidal particles (yellow) and soluble species (orange) in solution (blue). Reproduced with permission from ref 19. (D) Conceptual view of how the change in chemical potential ($\Delta\mu$) evolves with synthesis progress where $\Delta\mu$ is the difference in the chemical potentials between a particular zeolite phase (generically labeled I, II, and III) and an average value of the growth mixture (α and β) that accounts for sol gel heterogeneity.

ion exchange, impregnation, or chemical vapor deposition.[74−79]

A second class of SAS involves seed preservation, which typically occurs at relatively high seed content in zeolite growth mixtures; however, seed quantity is not the sole determinant of the SAS pathway. Unlike conventional crystallization systems where seeds are added to a supersaturated solution containing only monomers, the growth mixture in zeolite SAS is more complex (Figure 1B). The partitioning of silica and alumina into solution and solid phases creates a nonergodic medium where spatiotemporal variation of chemical potential dictates whether seeds grow or dissolve. In cases where seeds are the sole source of silica and alumina, the solution phase of the growth mixture is undersaturated and dissolution is often followed by IZT (*vide infra*). When seeds are preserved, growth may occur on the surface of the seed crystal to generate fins, core−shells, or nanosheets (Figure 2).[44,45,80−84] It is also possible that the surfaces of seed crystals provide an interface for heterogeneous nucleation.

Sacrificial SAS is the most reported case in the literature where seed dissolution is influenced by its composition (Si/Al ratio) based on the disparate rates of silica and alumina bond breakage.[85,86] It could be hypothesized that the memory of the parent pertains to a CBU; however, seeds are often metastable zeolites (e.g., FAU or BEA) that do not share CBUs with the final product. In cases where both parent and daughter are the same zeolite structure, evidence of CBUs produced during seed dissolution is generally lacking. An alternative explanation is that seed memory is the preservation of rings, although predicting synthesis outcomes based on ring size is indiscriminate given that most zeolites possess distributions of similar-sized rings. Oligomers generated from dissolving seeds could play a prominent role in SAS, which is consistent with Swaddle, who reported that acyclic species (e.g., dimers, trimers, etc.) are more reactive than cyclic species (e.g., rings or CBUs).[70] It is possible that more than one of these species (CBUs, rings, or oligomers) act in tandem, or perhaps there is a simpler explanation: the dissolved species promote the formation of the daughter phase by altering supersaturation, thereby lowering the energetic barrier for nucleation.

There are numerous benefits of seeding in zeolite synthesis beyond faster crystallization time or improved purity.[87] SAS can generate nanosized and hierarchical zeolites[18,45,78,88] (Figure 2) through facile routes that can also be used to tailor zeolite composition and framework structure. To this end, SAS has potential to be integrated into commercial production of zeolites in lieu of its economic feasibility. For instance, the use of zeolite seeds is more expensive than alternative aluminosilicate sources. This cost could be mitigated if a fraction of the product (daughter) is recycled;

https://doi.org/10.1021/jacs.1c11014
J. Am. Chem. Soc. 2021, 143, 21446−21460

however, few studies have explored multiple cycles to determine whether changes in recycled seed properties impact the products. A significant benefit of SAS is the potential to reduce or eliminate the use of OSDAs in synthesis mixtures. For example, Okubo and co-workers published a series of *green* synthesis studies (e.g., BEA[53] and MTW[54]) using a single recycling step as proof of principle for eliminating organics. In these processes the first stage to generate the initial batch of seeds may require organics, but subsequent batches can be performed OSDA-free, often at lower temperature than conventional methods, which improves synthesis efficiency and lowers energy costs. These factors, when coupled with the potential enhancement in zeolite physicochemical properties for applications, are significant advantages of SAS.

3. INTERZEOLITE TRANSFORMATIONS

The transformation from one zeolite framework to another can either occur by design using metastable zeolites as seeds (e.g., FAU and BEA), or it can be a direct outcome of organic-free synthesis. When seeds are used as the sole source of silica and alumina, their dissolution and subsequent nucleation of the daughter phase can be facilitated by the presence of an inorganic[89−97] or organic[45,93,98−109] structure-directing agent, a small quantity of seeds with identical structure as the daughter,[91,92,110,111] or in some cases neither seeds nor organics are required to achieve the desired product.[112,113] The role of inorganics in directing nucleation of the daughter phase was highlighted by Kirschhock and co-workers,[89] who reported transformations of Na-FAU seeds in growth mixtures containing four different alkali metals (Figure 3A), each promoting the formation of a different zeolite: Li-ABW, K-CHA, Cs-ANA, and Rb-MER. In some seed-assisted syntheses, IZT can dramatically reduce crystallization time,[68,114] such as a 3 day synthesis of K-CHA using zeolite HY (FAU) seeds compared to 14 days in the absence of seeds (for syntheses at 100 °C).[115] At different synthesis conditions, the same seeds (zeolite HY) can undergo IZT to Na-MFI (Figure 3B) in the absence of organics or MFI seeds.[112] It is common in organic-free synthesis that longer time and/or higher temperature can lead to multiple IZT events, such as the sequence of FAU-to-MFI-to-MOR shown in Figure 3B. The occurrence of impurities (e.g., quartz in Figure 3B) is also common, particularly when OSDAs are not used in syntheses to stabilize the daughter phase.[112]

IZT can provide pathways to synthesize zeolites with specific frameworks and/or compositions that are not possible with conventional silica and alumina sources. For example, B-SSZ-24 (AFI) has been synthesized by using a B-BEA precursor wherein the presence of BEA crystals in the growth mixture drives the system toward B-SSZ-24 crystallization,[116] which could not be achieved without zeolite seeds. Similarly, the aluminum-containing counterpart of VET (SSZ-41)[117] and high-silica ERI (SSZ-98)[118] were both achieved by using silica-rich FAU seeds. FAU-to-CHA IZT has been used to synthesize CHA zeolites with specific Al configurations (i.e., paired or isolated framework sites), wherein Al siting can impact zeolite catalyst performance in various chemical reactions.[119−121] Another application of IZT is the synthesis of metal-containing zeolites where hydrated metal precursors are too large to enter zeolite pore channels via traditional ion exchange. In this regard, zeolites with large pores (notably FAU) have been utilized as a carrier for metals to ensure their successful encapsulation in daughter crystals based on a ship-in-a-bottle approach where a parent zeolite stabilizes the metal clusters or nanoparticles in the interior preventing metal precipitation during synthesis of a medium- or small-pore zeolite (daughter) with high metal loading (Figure 2).[74,75] This approach was recently extended to the direct synthesis of phosphorus-containing AFX[122] and isomorphous substitution of metal ions in the zeolite framework.[77,123−126] Although literature on the subject of utilizing interzeolite transformations to create zeolites with different chemistry is relatively scarce, this could present new avenues for developing zeolites with unique properties for commercial applications.

Exploiting IZT in zeolite synthesis requires knowledge of factors influencing the specific sequence(s) of structural transformations and the resulting properties of the daughter phase. In classical crystallization, the growth unit is a single species (monomer) and the driving force for growth progressively decreases with a concomitant decrease in supersaturation. In zeolite synthesis, the sol gel (Figure 3C) is a complex growth medium wherein the concentration and speciation of (alumino)silicates partitioned between amorphous solid(s) and solution change as a function of time. This presumably leads to temporal changes in the chemical potential μ of both liquid (μ_1) and solid (μ_2) phases that favor the initial formation of a metastable parent; however, as the amorphous solid phase of the sol gel is depleted with time, the resulting supernatant imposes a driving force ($\Delta\mu$) that leads to the nucleation of a more thermodynamically stable daughter. Neglecting for the moment kinetic factors that may be responsible for nucleation of the daughter, a phenomenological representation of the thermodynamic argument in Figure 3D illustrates how IZT events among three generic zeolites (labeled I, II, and III) could occur when $\Delta\mu$ of the growth mixture (labeled as α) decreases with synthesis time. Once $\Delta\mu$ of the growth mixture reaches that of the metastable parent (zeolite I), there is a favorable $\Delta\mu$ between the supernatant and zeolite II that drives nucleation of the daughter (zeolite II) at the expense of dissolving parent crystals. This process can then be repeated for a subsequent transformation (zeolite II to III). It is theoretically possible that creating a synthesis mixture with a chemical potential equal to the supernatant of fully crystalline zeolite I and using this as the starting point (solution β) could bypass the first IZT sequence, leading to direct nucleation of zeolite II (as conceptualized in Figure 3D). This could result in a direct pathway to achieve more thermodynamically stable zeolites; however, a practical limitation of this approach may be a markedly reduced product yield if amorphous solids (i.e. majority of solute) must be removed from the growth mixture in order to achieve $\Delta\mu$ of solution β.

A key limitation of the concept depicted in Figure 3D is how to define (or quantify) the chemical potential of complex sol gel media. It is also uncertain to what degree the chemical potential of the amorphous solid and solution can be adjusted at the outset of synthesis to change the starting point, say from mixture α to β. There are many ways to alter the physicochemical properties of growth mixtures. For example, the selection of silica and/or alumina sources can impact zeolite crystallization[16,19,127−130] by altering properties such as the amorphous solid density and composition, the physical state of the sol gel (Figure 3C), and the partitioning of solute and its speciation between solid and liquid phases; however, it is less evident how these properties are directly linked to crystallization mechanisms. In nonseeded zeolite syntheses,

https://doi.org/10.1021/jacs.1c11014
J. Am. Chem. Soc. 2021, 143, 21446−21460

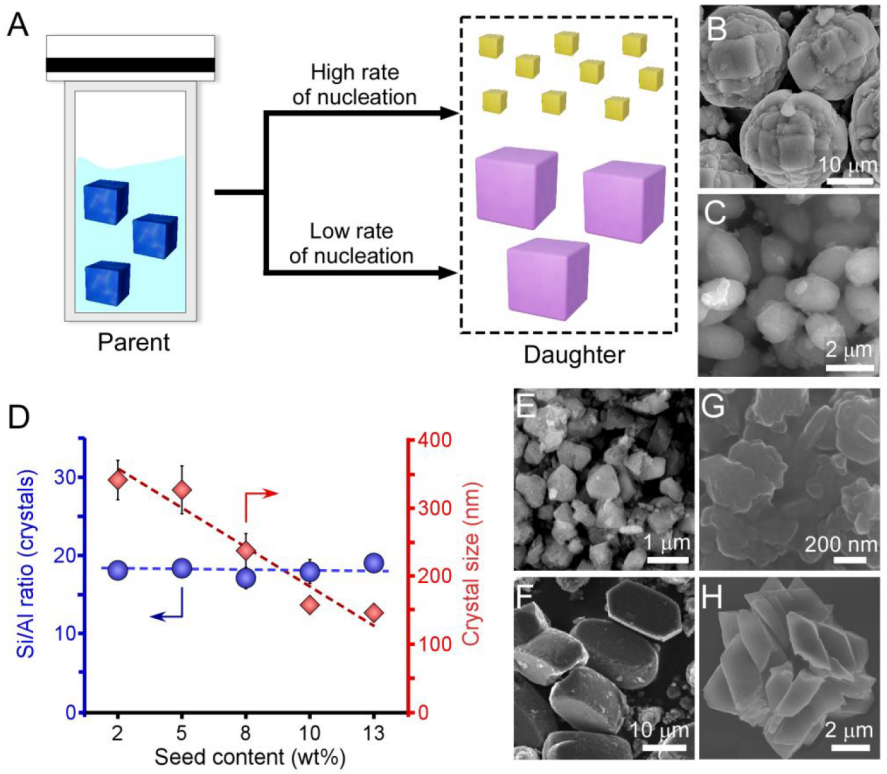

Figure 4. (A) Schematic highlighting two distinct effects where parent crystals (left) in a growth mixture lead to daughter crystals (right) of either smaller or larger size depending on the nucleation rate. (B, C) SEM images of ZSM-11 (MEL) crystals synthesized from identical synthesis mixtures (with diaminooctane as the OSDA) for (B) nonseeded and (C) seeded conditions where the product of the former is used as seeds for the latter. Reproduced with permission from ref 132. Copyright 2018 John Wiley and Sons. (D) Results of seeded ZSM-5 synthesis showing the impact of seed content on ZSM-5 product Si/Al ratio (blue circles) and crystal size (red diamonds). Error bars represent two standard deviations, and dashed lines are interpolations to guide the eye. Reproduced with permission from ref 86. Copyright 2020 Elsevier. (E–H) SEM images of parent–daughter crystals in two examples where IZT leads to large daughter crystal size: (E) parent USY (FAU) and (F) daughter ZSM-5 (MFI) crystals where USY seeds are utilized as the sole source of reagents. (E, F) Reproduced with permission from ref 112. Copyright 2019 John Wiley and Sons. (G) Parent FAU and (H) daughter GIS crystals from a nonseeded growth medium. (G, H) Reproduced with permission from ref 135. Copyright 2014 Royal Society of Chemistry.

silica concentrations are well in excess of amorphous silica solubility,[19] which generates an inhomogeneous growth medium where the majority of solute is contained within the amorphous solid. The chemical potential of the growth mixture presumably changes over the course of zeolite synthesis, which makes it difficult to correlate the driving force for zeolite crystallization to a single parameter such as supersaturation. While the rate of growth in classical crystallization decreases monotonically with depleted solute,[11] the supersaturation (or ΔC) in zeolite synthesis is difficult to define since the solute can be one of many species (i.e., monomers, oligomers, and amorphous solid). The relative contribution of each to the rate of nucleation is unknown; thus, developing models of zeolite crystallization would require a definition of chemical potential that reflects these complexities.

It is also less evident how chemical potential can be linked to synthesis conditions, such as solution pH, Si/Al ratio and solute speciation, and phase separation between amorphous solids/gels and solution. The change in chemical potential (or Gibbs free energy) during synthesis allows for use of phenomenological concepts, such as the Ostwald rule of stages,[131] to rationalize the sequences of IZT that occur with decreasing chemical potential (or increasing thermodynamic stability); however, predicting IZT sequences is nontrivial. For example, it is unclear why daughter zeolites in IZT often cannot form directly without the initial nucleation of a more metastable structure. A kinetic argument can be made on the basis of energetic barriers for nucleation, while a thermodynamic argument can be made on the basis of chemical potential (Figure 3D) wherein the evolved growth mixture provides a more favorable environment for the nucleation of the daughter phase. This poses a question: is it possible to bypass IZT by altering the initial growth conditions in ways that lower energetic barriers and/or change chemical potential to favor direct synthesis of more thermodynamically stable zeolites?

4. IMPACT OF SEEDS ON CRYSTAL SIZE AND PURITY

One advantage of sacrificial seeding is enhanced nucleation of the daughter phase to produce smaller crystals than those obtained by direct synthesis (Figure 4A). This can be influential in situations where alternative modifications to synthesis conditions (e.g., composition, temperature, etc.) may not be feasible. For instance, the synthesis of ZSM-11 (MEL) often contains ZSM-5 (MFI) as an impurity when tetrabutylammonium (TBA) is used as the OSDA. Replacement with diaminooctane (DAO) yields a pure MEL product, but the crystals are large (ca. 20 μm, Figure 4B) compared to those obtained in TBA-based syntheses (<1 μm).[132] However, it was shown that using the large ZSM-11 crystals as seeds in the DAO-based growth mixture results in crystals with sizes that

https://doi.org/10.1021/jacs.1c11014
J. Am. Chem. Soc. 2021, 143, 21446–21460

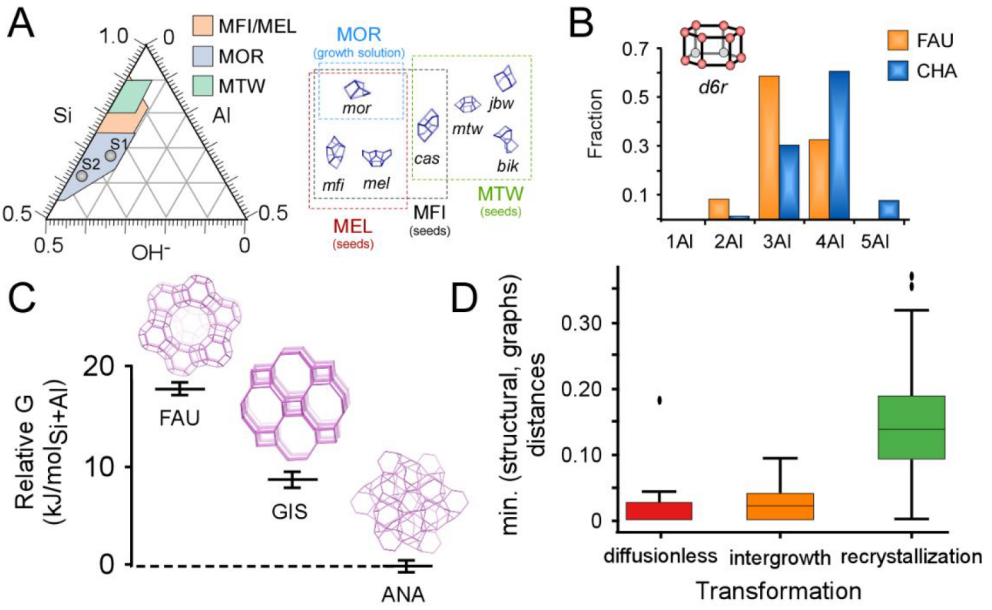

Figure 5. (A) Relationships among MFI, MEL, MOR, and MTW synthesis conditions (left) and framework structures (right). The kinetic ternary phase diagram depicts which synthesis compositions (molar fractions of Si, Al, and OH) promote each structure with two specific growth mixtures (labeled S1 and S2). The Venn diagram of composite building units for each framework indicate overlapping structural similarities. Reproduced with permission from ref 86. Copyright 2020 Elsevier. (B) Composition of double-six-membered rings (*d6r*, inset) from ^{29}Si MAS NMR analysis of FAU (parent) to CHA (daughter) IZT. The noticeable shift in composition toward higher numbers of Al atoms per CBU indicates that *d6r* building units do not remain intact throughout the transformation. Figure created by using data from ref 120. (C) Relative Gibbs free energies of three zeolite phases (FAU, GIS, and ANA) in an IZT sequence that follows the Ostwald rule of stages. The zeolite free energy is estimated by using Metropolis Monte Carlo simulations of structures with composition Si/Al = 2. Framework structures of original replaced for consistency. Reproduced with permission from ref 139. Copyright 2019 Nature Research. (D) Graphical parent−daughter relationships between known IZTs for different mechanisms. Transformations occurring via diffusionless (or topotactic) mechanisms typically involve two structures with high graph similarity according to the SOAP method. Reproduced with permission from ref 140. Copyright 2019 Nature Publishing Group.

are an order of magnitude smaller (Figure 4C). Similar examples have been reported for other zeolites where the memory of the dissolving seed seemingly promotes the rate of nucleation.[88,133,134] This was observed in a study of seeded ZSM-5 synthesis where the final crystal size monotonically decreases with increased seed weight percent (Figure 4D).[86] When the percentage of seeds in the growth mixture becomes relatively large, the trend can potentially be shifted to produce daughter crystals with larger size (Figure 4A). This has been observed when a metastable zeolite is used as the sole source of silica and alumina, and prolonged seed dissolution leads to reduced rates of nucleation of the daughter phase. For example, the use of zeolite USY seeds (Figure 4E) to produce ZSM-5 crystals (Figure 4F) resulted in much larger particles compared to most nonseeded syntheses of ZSM-5. An analogous situation is encountered in IZT where the majority of solute (Si and Al) is often contained within the parent zeolite compared to the supernatant solution. One example is the FAU-to-GIS transition[55,135] where the size of parent crystals (Figure 4G) is markedly smaller than that of the daughter (Figure 4H).

The weight percentage of parent crystals in SAS (or IZT) compared to the total quantity of reagent in the growth mixture is not a universal indicator of the pathway leading to either smaller or larger daughter crystal size. Trends in Figure 4 could depend on whether species involved in nucleation are principally derived from solution or the amorphous solid. In cases where the parent crystal accounts for most of total silica and alumina content, nucleation of the daughter occurs in media without an appreciable number of amorphous precursors; thus, nucleation predominantly involves soluble species and/or fragments of dissolving parent crystals. In cases where the seed percentage is relatively low, nucleation occurs in media with a larger quantity of amorphous precursors. It is possible that either of these scenarios could lead to higher rates of daughter nucleation depending on the nature of the system being studied.

5. GENERALIZED GUIDELINES

There are currently no theoretical models capable of predicting seed-assisted and interconversion pathways, but heuristic guidelines have been hypothesized to rationalize causal relationships between parent−daughter frameworks, growth solution composition, and other synthesis conditions. Examples of general guidelines include a hypothesis for seed-assisted syntheses[64] positing a daughter will crystallize with the same framework as the parent when the seed shares at least one common CBU with the zeolite obtained from the same synthesis mixture without seeds. This has been observed in a number of cases.[58,110,111,136−138] For example, Okubo and coworkers[64,87] showed that ZSM-11 (MEL) seeds introduced in a mordenite (MOR) growth mixture yield a ZSM-11 product. The synthesis composition selected for that study is represented as solution S2 in Figure 5A, which falls well within the pure MOR phase region. The common CBU shared by MEL and MOR (*mor* in Figure 5A) putatively enables the growth of MEL outside of its phase region in the ternary diagram. A similar case was reported[64] for zeolite ZSM-5 (MFI) seeds in a mordenite (MOR) growth mixture (solution S2, Figure 5A), which yields a ZSM-5 product. This case aligns

https://doi.org/10.1021/jacs.1c11014
J. Am. Chem. Soc. 2021, 143, 21446−21460

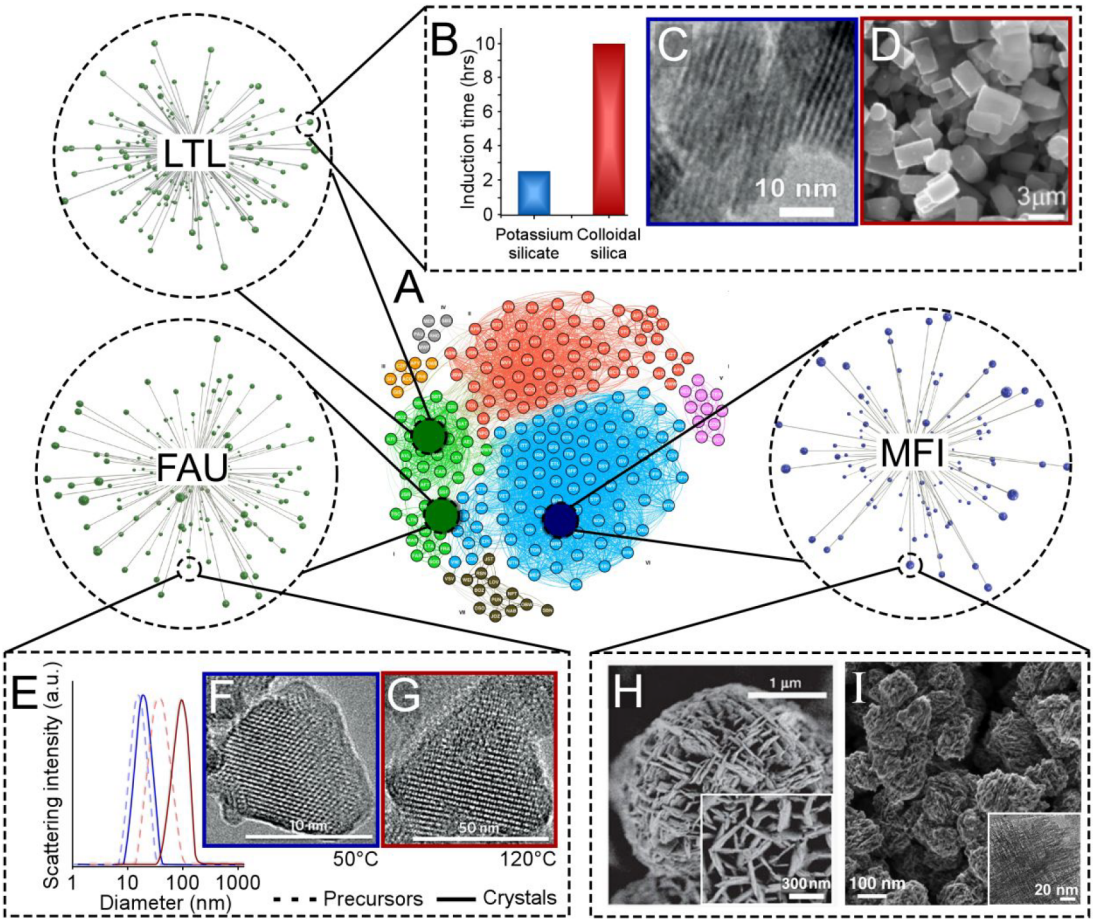

Figure 6. (A) Machine learning network of synthetically realized zeolites where nodes are connected based on structural similarity and seven communities (color-coded) are identified based on a clustering algorithm. Callouts added to original. Reproduced with permission from ref 139. Copyright 2019 Nature Research. Callouts: examples from the literature are highlighted to conceptualize numerous nodes that factor into the synthesis of each framework and dictate physicochemical properties (e.g., size, morphology, composition, and crystallinity). It remains unclear to what extent findings for modifying crystals of one framework type (locally) can be extended to other structures (globally). (B–D) Changes in silica source can alter the induction time (B) and crystal size (C, D) in zeolite L (LTL) syntheses. Reproduced with permission from ref 144. Copyright 2018 John Wiley and Sons. (E–G) Particle size distribution (E) and representative TEM images of zeolite Y (FAU) crystals synthesized from a precursor solution mixed in an ice bath and synthesized at (F) 50 °C for 45 h (blue) and (G) 120 °C for 70 min (red). Reproduced with permission from ref 145. Copyright 2015 Nature Publishing Group. (H, I) SEM images of hierarchical MFI synthesized with distinct OSDAs: (H) nanosheets where a bifunctional surfactant obstructs growth along the *b* direction. Reproduced with permission from ref 146. Copyright 2009 Springer Nature. (I) Purely siliceous self-pillared pentasil prepared with tetrabutylphosphonium to promote nanoscopic MEL intergrowths. Inset: TEM image revealing the mesoporous nature of pillared crystals. Reproduced with permission from ref 147. Copyright 2012 AAAS.

with the CBU hypothesis since ZSM-5 and mordenite share a *mor* building unit (Figure 5A); however, this study also revealed that the outcome depends upon various conditions that include seed Si/Al ratio, growth mixture composition, and synthesis time.[86] For instance, a ZSM-5 product in solution S2 was only obtained at intermediate seed Si/Al ratio and short periods of hydrothermal treatment. Prolonged synthesis time resulted in an MFI-to-MOR interzeolite transformation. Moreover, switching the growth medium to solution S1 (Figure 5A), which is also within the MOR phase region, resulted in a mordenite product irrespective of seed composition. The same study also assessed the use of seeds, such as ZSM-12 (MTW) which lacks a common CBU with mordenite. At short synthesis times, solutions S1 and S2 yield ZSM-5 and ZSM-12 products, respectively. At longer synthesis time, a similar IZT sequence leading to MOR as the product is observed in both solutions. What can be gleaned from studies testing the hypothesis of common CBUs is that it is a general guideline for many cases, specifically at short synthesis times, but it is not a universal heuristic.

Hypotheses of common CBUs have also been invoked to rationalize sequences of interzeolite transformation; however, there are a number of reported cases where parent and daughter lack a common CBU.[110,112] In cases where parent–daughter structural similarities exist, it was shown by Okubo and co-workers[120] for the FAU-to-CHA transformation that the common CBU (double-six-membered ring, *d6r*) exhibits a shift in the number of Al sites per *d6r* (Figure 5B), which indicates the CBU is not directly transferred from a dissolving parent to a growing daughter crystal. It is also challenging to draw upon more generalizable structural features, such as ring building units (RBUs) and secondary building units (SBUs),[67] which are underspecified descriptors for deriving causal relationships between parent and daughter crystals. A more general descriptor of IZT sequences is the Gibbs free energy, ΔG. Okubo and co-workers used Metropolis Monte Carlo simulations to estimate the free energies of 23 different zeolite

https://doi.org/10.1021/jacs.1c11014
J. Am. Chem. Soc. 2021, 143, 21446–21460

structures, illustrating that ΔG can be used to explain—but not predict—IZT sequences (Figure 5C).[139] Interestingly, their model captures variations in relative free energy with framework Si/Al ratio; however, models of ΔG are not fully developed as many either neglect or cannot accurately account for factors such as solvent (e.g., water) that are necessary to capture entropic contributions. Proxy variables for ΔG have also been used to describe IZT. For example, Navrotsky and co-workers[141] reported that enthalpy of formation, ΔH_f, for all-silica zeolites is proportional to the molar volume of the zeolite framework. The latter has been used to rationalize IZT sequences among aluminosilicates[55] where the trend is valid for many cases, such as FAU-to-GIS-to-ANA in Figure 5C, but not for others (e.g., MFI-to-MOR in Figure 3B).[112] This is not unexpected given that Navrotsky and Petrovic[142] also showed that ΔH_f is strongly dependent upon the Si/Al ratio of the zeolite framework, consistent with Sano and co-workers[72] reporting that the presence of Al can alter dissolution rates (i.e., stability) of a parent zeolite irrespective of its framework density. These collective studies highlight the challenges of identifying a single property of zeolites capable of rationalizing IZT sequences.

Advancements in computational analysis of zeolite syntheses have led to mathematical models classifying interzeolite transformations and predicting relationships between frameworks. Gómez-Bombarelli and co-workers[140] used a methodology known as smooth overlap of atomic positions (SOAP) to quantify and map structural similarities between different framework topologies. They correlate the graphical distance between two frameworks (plotted in the *y*-axis of Figure 5D as the minimum distance) as calculated by the SOAP method with the type of IZT likely to occur between zeolite structures. They demonstrated that a high degree of graph similarity is an excellent predictor of which parent−daughter pairs can participate in IZT classes that require two complementary structures, such as diffusionless (topotactic) or (epitaxial) intergrowth, whereas for recrystallization the parent largely decomposes prior to daughter nucleation. Their detailed investigation into graph similarity highlights that framework similarity among zeolites is likely more complex than the identification of common rings, building units, or (half) tiles.[143] Okubo and co-workers[139] used machine learning (ML) to create a similarity network of zeolite frameworks (Figure 6A). Rather than using mathematically modeled crystal lattices, however, their ML algorithm was trained based on synthesis gel components and compositions. These examples reveal how descriptors based on rigorous analysis of zeolite syntheses—compared to general properties (e.g., CBUs and molar volume)—offer potential for predicting synthesis outcomes. One challenge related to *in silico* approaches is that IZT sequences in experimental studies are potentially overlooked, and hence not reported, when only the end-product is evaluated without carrying out time-resolved measurements of various stages during zeolite synthesis.

6. IS THERE A NETWORK THEORY FOR ZEOLITE SYNTHESIS?

The advent of machine learning and data analytics has created new opportunities to guide SAS and IZT by identifying similarities in zeolite structures,[140] relationships between synthesis conditions and zeolite properties,[139] and insight into the selection of structure-directing agents.[148] The similarity network developed for zeolite structures in Figure 6A is composed of clusters (or modules) where each color represents a similar topology based on secondary and composite building units.[139] It has been suggested that similarity networks could be applied to zeolite synthesis as a way of drawing connections between multiple nodes, such as crossover synthesis experiments where conditions for one zeolite could potentially be applied to another. Here we pose a more general question: is there a global synthesis network based on fundamental similarities for controlling zeolite nucleation and growth? To explore this concept, we discuss herein three different approaches to synthesize nanosized or hierarchical zeolites for three nodes on the structure similarity network: LTL, FAU, and MFI. The first approach demonstrated for zeolite L (LTL) involves the judicious selection of a silica source wherein it was shown that the replacement of colloidal silica (or fumed silica) with potassium silicate dramatically reduces nucleation induction time (Figure 6B) and crystal size (Figure 6C,D).[144] For the synthesis of zeolite Y (FAU) it has been reported that low temperature during the mixing of reagents inhibits the aggregation of amorphous precursors (Figure 6E), thereby increasing the number of nuclei and producing ultrasmall zeolite particles of ca. 10 nm (Figure 6F) compared to conventional syntheses (Figure 6G).[145] In the third example, multiple groups have shown that appropriate selection of an OSDA can lead to the synthesis of MFI nanosheets (Figure 6H) and self-pillared (Figure 6I) structures.[146,147] In all three examples there is a different parameter being adjusted for each framework type (i.e., silica source, temperature, and OSDA), but the ability to draw connections between each node relies on understanding how these parameters influence zeolite nucleation on a fundamental level. For example, a crossover synthesis using low-temperature mixing for ZSM-5 may not result in an identical effect as zeolite Y, whereas the basic concept of altering the size or colloidal stability of precursors may be the true connection where the means to accomplish these ends involves the manipulation of different synthesis parameters. Examples of successful translational concepts include adaptations of the surfactant-based OSDA used to obtain MFI nanosheets (Figure 6H). Román-Leshkov and co-workers[149] used a similar construct to prepare two-dimensional MCM-22 (MWW), whereas Ryoo and co-workers[150] used organosilanes as OSDA analogues to produce similar outcomes for FAU, CHA, and MOR with the assistance of seeding.

Recent machine learning analyses coupled with decades of experimental studies[139,148,151−154] have taught us that a single parameter is an insufficient predictor of outcomes in zeolite synthesis. Rather, multiple factors must be considered when trying to correlate the effects of synthesis parameters to SAS and IZT. Temperature is one of the most impactful parameters, not only during the initial mixing of reagents but also during hydrothermal treatment where numerous studies have shown that low temperatures favor nucleation over crystal growth, thus leading to nanosized crystals.[155] In contrast, higher temperature can provide the energy required to overcome barriers for interzeolite transformations.[55] For certain seed-assisted syntheses, an OSDA is most critical to achieving the desired product, whereas for nonseeded syntheses, IZT tends to occur more readily in organic-free syntheses containing alkali and/or alkaline earth metals. Substitution of different heteroatoms (e.g., Ge) can also play a significant role in zeolite crystallization by introducing sites that more readily dissolve for SAS, IZT, and other processes

https://doi.org/10.1021/jacs.1c11014
J. Am. Chem. Soc. 2021, 143, 21446−21460

(e.g., ADOR).[156,157] Dissolution (bond breaking) and condensation (bond forming) also rely on the concentration of mineralizing agents, such as hydroxide or fluoride ions.[58,158−161] Indeed, the list can be extended to a myriad of synthesis parameters where the answer to the question of whether synthesis outcomes can be related to a global network connecting many nodes (or clusters) relies on the ability to identify causal relationships that go beyond synthesis parameters to their specific, fundamental impact on zeolite nucleation and growth. How do synthesis parameters alter solute speciation, supersaturation, precursor/seed dissolution rates, sol−gel composition and heterogeneities, and dynamic changes to each of these variables over the course of synthesis? Also, how generalizable are observations for one zeolite to diverse framework types and synthesis conditions? Answering these questions has the potential to provide connections between nodes in an idealized network of zeolite syntheses toward translating shared outcomes across a spectrum of materials, analogous to those highlighted in Figure 6. There are previous studies that serve as models toward answering the questions posed above, such as the work of Wakihara and co-workers,[127] who comparatively investigated the effect of different silica sources on the structural evolution of amorphous precursors and established a link between the reactivity of reactants, condensation kinetics, and zeolite nucleation.

7. SUMMARY AND OUTLOOK

In this Perspective we discuss conceptual approaches toward establishing causal relationships between synthesis conditions and zeolite properties. There are numerous synthesis parameters that can be manipulated, but linking the effects of each to synthesis outcomes is not an easy task—one made even more difficult by the complexity of the sol gel media. Many open-ended questions posed here are nebulous, such as how to define the amorphous state of precursors and how to select descriptors (e.g., chemical potential) that represent the driving force for zeolite crystallization. The analogy in section 6 to neural-like networks puts forward a grand challenge in zeolite synthesis where the degree to which connections can be made among the >250 known framework types remains to be determined. If we compare zeolites with other classes of crystals that grow exclusively by a classical pathway, one advantage of latter systems is that the primary growth unit can be monitored over the course of crystallization. This allows models based on supersaturation and other measurable variables to predict nucleation and growth rates with acceptable accuracy. In zeolite synthesis, the diversity of species and the dynamic changes in their concentration and/or structure make it difficult to develop universal models of crystallization.

Here we discuss many examples where seed-assisted synthesis and interzeolite transformations provide greater flexibility in the design of zeolites. The most pervasive question in these processes is, what species (or memory) of dissolving parent material are instrumental for promoting nucleation of the daughter? If the primary goal in SAS, IZT, and other methods of zeolite synthesis is to produce smaller crystals, greater emphasis should be placed on studying aspects of nucleation—a topic that is challenging on several levels. The physical state of growth media, such as heterogeneity and high solid concentrations (i.e., viscous or opaque mixtures), makes it difficult for *in situ* characterization. Another complicating factor is that zeolite nucleation is rapid in comparison to much longer induction times. For example, time-resolved SEM images of solids extracted from a typical zeolite L (LTL) synthesis reveal amorphous precursors after 4 h of hydrothermal treatment (Figure 7A), consistent with the powder X-ray diffraction (PXRD) pattern showing no evidence of crystallinity.[30] A sample extracted after 8 h, prior to the onset of Bragg peaks in PXRD patterns, contains zeolite L crystals (Figure 7B) with sizes nearly equivalent to those of the final product after complete crystallization. This exemplifies most situations encountered in zeolite synthesis where the ability to quench syntheses and visualize stages of nucleation is challenging. In many cases, once crystals form their growth is rapid. This is exemplified in SSZ-13 (CHA) syntheses where samples extracted after PXRD patterns show the first signs of Bragg peaks (Figure 7C) contain large crystals (labeled i) surrounded by amorphous precursors (labeled ii).[159] High-resolution transmission electron micrographs of these SSZ-13 crystals (Figure 7D) show evidence of nonclassical growth by particle attachment (i.e., protrusions iii with sizes comparable to amorphous precursors) as well as smaller features (iv in Figure 7D) that are putative intermediates during the disorder-to-order transition of adsorbed precursors as they integrate into the underlying crystal. The ability to capture similar images of nuclei by electron microscopy has remained elusive, with the images highlighted in Figure 1C−F being among the few exceptions. An approach that may be generally applicable to a broader set of zeolites is one used by Tsapatsis and co-

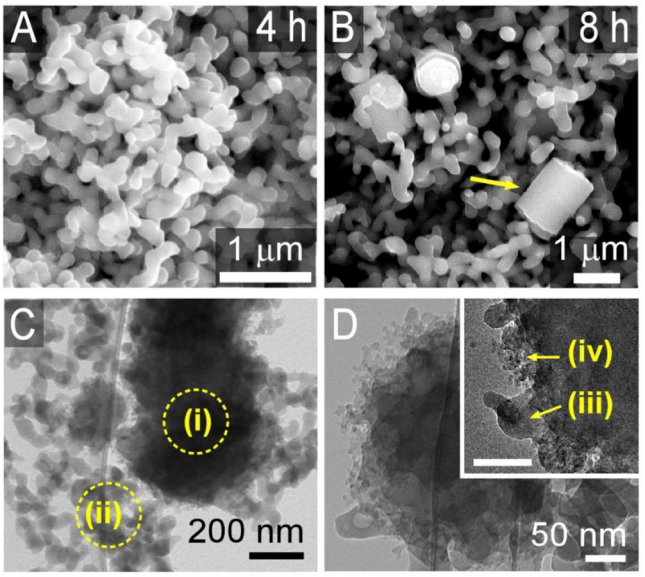

Figure 7. (A, B) SEM images of solids extracted from a zeolite L synthesis after (A) 4 h and (B) 8 h of hydrothermal treatment. The samples are composed of amorphous precursors with zeolite L crystals (arrow) apparent at the later time. Reproduced with permission from ref 30. (C, D) TEM images of solids extracted from a SSZ-13 synthesis at a time corresponding to the first evidence of Bragg peaks in PXRD patterns. (C) Low-magnification image showing populations of crystals (i) and amorphous precursors (ii). (D) High-magnification image showing evidence of crystallization by particle attachment. Inset: image of a crystal surface with protrusions (iii) equivalent to the size of amorphous precursors and smaller particles (iv) that are putative intermediates of the disorder-to-order transition. Reproduced with permission from ref 159.

https://doi.org/10.1021/jacs.1c11014
J. Am. Chem. Soc. 2021, 143, 21446−21460

workers for silicalite-1 where the image of the nucleus shown in Figure 1C was taken after nearly one year of synthesis at room temperature.[15] The reduction of synthesis temperature to a point where nucleation occurs at exceptionally long time scales could allow for similar analyses of other zeolite framework types, albeit requiring extraordinary patience on behalf of researchers.

Future development of seed-assisted and other methods in zeolite synthesis would greatly benefit from more in-depth knowledge of fundamental mechanisms. This, in turn, places more emphasis on experimental studies to go beyond observational findings—where changes to a synthesis parameter are correlated to a modified property of the zeolite—toward efforts that address how changes to each synthesis parameter alter the physicochemical state of the system and its corresponding impact on nucleation and/or growth. Examples have already demonstrated how partial answers to these questions can be achieved from the synergy of combined experimental and computational efforts. The neural network concept for zeolite synthesis may potentially be realized with the aid of machine learning and data analytics. Similar approaches have been applied to other materials, such as polymers, metal−organic frameworks, and semiconductors.[162−166] The emergence of new tools such as these may prove instrumental for the translation of zeolite synthesis methods across a broad set of crystal structures and synthesis conditions.

AUTHOR INFORMATION

Corresponding Author

Jeffrey D. Rimer − *Department of Chemical and Biomolecular Engineering, University of Houston, Houston, Texas 77204, United States;* orcid.org/0000-0002-2296-3428; Email: jrimer@central.uh.edu

Authors

Rishabh Jain − *Department of Chemical and Biomolecular Engineering, University of Houston, Houston, Texas 77204, United States;* orcid.org/0000-0001-5748-5932

Adam J. Mallette − *Department of Chemical and Biomolecular Engineering, University of Houston, Houston, Texas 77204, United States*

Complete contact information is available at: https://pubs.acs.org/10.1021/jacs.1c11014

Notes

The authors declare no competing financial interest.

ACKNOWLEDGMENTS

This work was primarily supported by the National Science Foundation (Awards DMR-2005201 and DMREF-1629398). Additional support was provided by The Welch Foundation (E-1794).

REFERENCES

(1) Zhang, R.; Liu, N.; Lei, Z.; Chen, B. Selective transformation of various nitrogen-containing exhaust gases toward N_2 over zeolite catalysts. *Chem. Rev.* **2016**, *116* (6), 3658−3721.

(2) Beale, A. M.; Gao, F.; Lezcano-Gonzalez, I.; Peden, C. H.; Szanyi, J. Recent advances in automotive catalysis for NOx emission control by small-pore microporous materials. *Chem. Soc. Rev.* **2015**, *44* (20), 7371−7405.

(3) Gao, P.; Li, S.; Bu, X.; Dang, S.; Liu, Z.; Wang, H.; Zhong, L.; Qiu, M.; Yang, C.; Cai, J.; Wei, W.; Sun, Y. Direct conversion of CO_2 into liquid fuels with high selectivity over a bifunctional catalyst. *Nat. Chem.* **2017**, *9* (10), 1019−1024.

(4) Jae, J.; Tompsett, G. A.; Foster, A. J.; Hammond, K. D.; Auerbach, S. M.; Lobo, R. F.; Huber, G. W. Investigation into the shape selectivity of zeolite catalysts for biomass conversion. *J. Catal.* **2011**, *279* (2), 257−268.

(5) Ennaert, T.; Van Aelst, J.; Dijkmans, J.; De Clercq, R.; Schutyser, W.; Dusselier, M.; Verboekend, D.; Sels, B. F. Potential and challenges of zeolite chemistry in the catalytic conversion of biomass. *Chem. Soc. Rev.* **2016**, *45* (3), 584−611.

(6) Mark, L. O.; Cendejas, M. C.; Hermans, I. The use of heterogeneous catalysis in the chemical valorization of plastic waste. *ChemSusChem* **2020**, *13* (22), 5808−5836.

(7) Liu, S.; Kots, P. A.; Vance, B. C.; Danielson, A.; Vlachos, D. G. Plastic waste to fuels by hydrocracking at mild conditions. *Sci. Adv.* **2021**, *7* (17), eabf8283.

(8) Vermeiren, W.; Gilson, J.-P. Impact of zeolites on the petroleum and petrochemical industry. *Top. Catal.* **2009**, *52* (9), 1131−1161.

(9) Vogt, E. T.; Whiting, G. T.; Chowdhury, A. D.; Weckhuysen, B. M. Zeolites and zeotypes for oil and gas conversion. *Adv. Catal.* **2015**, *58*, 143−314.

(10) Kalikmanov, V. I. Classical Nucleation Theory. In *Nucleation Theory*; Springer Netherlands: Dordrecht, 2013; pp 17−41.

(11) De Yoreo, J. J.; Vekilov, P. G. Principles of crystal nucleation and growth. *Rev. Mineral. Geochem.* **2003**, *54* (1), 57−93.

(12) De Yoreo, J. A Perspective on Multistep Pathways of Nucleation. In *Crystallization via Nonclassical Pathways*; American Chemical Society: 2020; Vol. *1*, pp 1−17.

(13) Vekilov, P. G. Nonclassical Nucleation. In *Crystallization via Nonclassical Pathways*; American Chemical Society: 2020; Vol. *1*, pp 19−46.

(14) Vekilov, P. G. The two-step mechanism of nucleation of crystals in solution. *Nanoscale* **2010**, *2* (11), 2346−2357.

(15) Davis, T. M.; Drews, T. O.; Ramanan, H.; He, C.; Dong, J.; Schnablegger, H.; Katsoulakis, M. A.; Kokkoli, E.; McCormick, A. V.; Penn, R. L.; Tsapatsis, M. Mechanistic principles of nanoparticle evolution to zeolite crystals. *Nat. Mater.* **2006**, *5* (5), 400−408.

(16) Oleksiak, M. D.; Soltis, J. A.; Conato, M. T.; Penn, R. L.; Rimer, J. D. Nucleation of FAU and LTA zeolites from heterogeneous aluminosilicate precursors. *Chem. Mater.* **2016**, *28* (14), 4906−4916.

(17) Mintova, S.; Olson, N. H.; Valtchev, V.; Bein, T. Mechanism of zeolite A nanocrystal growth from colloids at room temperature. *Science* **1999**, *283* (5404), 958−960.

(18) Jain, R.; Chawla, A.; Linares, N.; García Martínez, J.; Rimer, J. D. Spontaneous pillaring of pentasil zeolites. *Adv. Mater.* **2021**, *33* (22), 2100897.

(19) Li, R.; Chawla, A.; Linares, N.; Sutjianto, J. G.; Chapman, K. W.; Martínez, J. G.; Rimer, J. D. Diverse Physical States of Amorphous Precursors in Zeolite Synthesis. *Ind. Eng. Chem. Res.* **2018**, *57* (25), 8460−8471.

(20) Bibby, D.; Dale, M. Synthesis of silica-sodalite from non-aqueous systems. *Nature* **1985**, *317* (6033), 157−158.

(21) Parnham, E. R.; Morris, R. E. Ionothermal synthesis of zeolites, metal−organic frameworks, and inorganic−organic hybrids. *Acc. Chem. Res.* **2007**, *40* (10), 1005−1013.

(22) Cooper, E. R.; Andrews, C. D.; Wheatley, P. S.; Webb, P. B.; Wormald, P.; Morris, R. E. Ionic liquids and eutectic mixtures as solvent and template in synthesis of zeolite analogues. *Nature* **2004**, *430* (7003), 1012−1016.

(23) Ma, H.; Tian, Z.; Xu, R.; Wang, B.; Wei, Y.; Wang, L.; Xu, Y.; Zhang, W.; Lin, L. Effect of water on the ionothermal synthesis of molecular sieves. *J. Am. Chem. Soc.* **2008**, *130* (26), 8120−8121.

(24) Tian, Y.; McPherson, M. J.; Wheatley, P. S.; Morris, R. E. Ionic Liquid assisted Synthesis of Zeolite-TON. *Z. Anorg. Allg. Chem.* **2014**, *640* (6), 1177−1181.

(25) Matsukata, M.; Ogura, M.; Osaki, T.; Rao, P. R. H. P.; Nomura, M.; Kikuchi, E. Conversion of dry gel to microporous crystals in gas phase. *Top. Catal.* **1999**, *9* (1), 77−92.
(26) Wu, Q.; Meng, X.; Gao, X.; Xiao, F.-S. Solvent-free synthesis of zeolites: mechanism and utility. *Acc. Chem. Res.* **2018**, *51* (6), 1396−1403.
(27) Ren, L.; Wu, Q.; Yang, C.; Zhu, L.; Li, C.; Zhang, P.; Zhang, H.; Meng, X.; Xiao, F.-S. Solvent-free synthesis of zeolites from solid raw materials. *J. Am. Chem. Soc.* **2012**, *134* (37), 15173−15176.
(28) Jin, Y.; Sun, Q.; Qi, G.; Yang, C.; Xu, J.; Chen, F.; Meng, X.; Deng, F.; Xiao, F. S. Solvent-free synthesis of silicoaluminophosphate zeolites. *Angew. Chem., Int. Ed.* **2013**, *52* (35), 9172−9175.
(29) Kumar, S.; Davis, T. M.; Ramanan, H.; Penn, R. L.; Tsapatsis, M. Aggregative growth of silicalite-1. *J. Phys. Chem. B* **2007**, *111* (13), 3398−3403.
(30) Kumar, M.; Li, R.; Rimer, J. D. Assembly and evolution of amorphous precursors in zeolite L crystallization. *Chem. Mater.* **2016**, *28* (6), 1714−1727.
(31) Mintova, S.; Olson, N. H.; Bein, T. Electron microscopy reveals the nucleation mechanism of zeolite Y from precursor colloids. *Angew. Chem., Int. Ed.* **1999**, *38* (21), 3201−3204.
(32) Serrano, D.; Uguina, M.; Ovejero, G.; Van Grieken, R.; Camacho, M. Evidence of solid-solid transformations during the TS-1 crystallization from amorphous wetness impregnated SiO_2—TiO_2 xerogels. *Microporous Mater.* **1996**, *7* (6), 309−321.
(33) Valtchev, V. P.; Bozhilov, K. N. Transmission electron microscopy study of the formation of FAU-type zeolite at room temperature. *J. Phys. Chem. B* **2004**, *108* (40), 15587−15598.
(34) Hould, N. D.; Kumar, S.; Tsapatsis, M.; Nikolakis, V.; Lobo, R. F. Structure and colloidal stability of nanosized zeolite beta precursors. *Langmuir* **2010**, *26* (2), 1260−1270.
(35) Ren, N.; Subotić, B.; Bronić, J.; Tang, Y.; Dutour Sikirić, M.; Mišić, T.; Svetličić, V.; Bosnar, S.; Antonić Jelić, T. Unusual pathway of crystallization of zeolite ZSM-5 in a heterogeneous system: phenomenology and starting considerations. *Chem. Mater.* **2012**, *24* (10), 1726−1737.
(36) Valtchev, V. P.; Bozhilov, K. N. Evidences for zeolite nucleation at the solid−liquid interface of gel cavities. *J. Am. Chem. Soc.* **2005**, *127* (46), 16171−16177.
(37) Valtchev, V.; Rigolet, S.; Bozhilov, K. N. Gel evolution in a FAU-type zeolite yielding system at 90 C. *Microporous Mesoporous Mater.* **2007**, *101* (1−2), 73−82.
(38) Nikolakis, V.; Vlacho, D. G.; Tsapatsis, M. Modeling of zeolite crystallization: the role of gel microstructure. *Microporous Mesoporous Mater.* **1998**, *21* (4−6), 337−346.
(39) Yamada, H.; Tominaka, S.; Ohara, K.; Liu, Z.; Okubo, T.; Wakihara, T. Structural Evolution of Amorphous Precursors toward Crystalline Zeolites Visualized by an in Situ X-ray Pair Distribution Function Approach. *J. Phys. Chem. C* **2019**, *123* (46), 28419−28426.
(40) Larlus, O.; Valtchev, V. P. Crystal morphology control of LTL-type zeolite crystals. *Chem. Mater.* **2004**, *16* (17), 3381−3389.
(41) Evans, A. M.; Parent, L. R.; Flanders, N. C.; Bisbey, R. P.; Vitaku, E.; Kirschner, M. S.; Schaller, R. D.; Chen, L. X.; Gianneschi, N. C.; Dichtel, W. R. Seeded growth of single-crystal two-dimensional covalent organic frameworks. *Science* **2018**, *361* (6397), 52−57.
(42) Smith, J. D.; Scanlan, M. M.; Chen, A. N.; Ashberry, H. M.; Skrabalak, S. E. Kinetically controlled sequential seeded growth: A general route to crystals with different hierarchies. *ACS Nano* **2020**, *14* (11), 15953−15961.
(43) Xu, H.-Q.; Wang, K.; Ding, M.; Feng, D.; Jiang, H.-L.; Zhou, H.-C. Seed-mediated synthesis of metal−organic frameworks. *J. Am. Chem. Soc.* **2016**, *138* (16), 5316−5320.
(44) Dai, H.; Shen, Y.; Yang, T.; Lee, C.; Fu, D.; Agarwal, A.; Le, T. T.; Tsapatsis, M.; Palmer, J. C.; Weckhuysen, B. M.; Dauenhauer, P. J.; Zou, X.; Rimer, J. D. Finned zeolite catalysts. *Nat. Mater.* **2020**, *19* (10), 1074−1080.
(45) Ding, K.; Corma, A.; Maciá-Agulló, J. A.; Hu, J. G.; Krämer, S.; Stair, P. C.; Stucky, G. D. Constructing hierarchical porous zeolites via kinetic regulation. *J. Am. Chem. Soc.* **2015**, *137* (35), 11238−11241.
(46) Hou, L.-Y.; Thompson, R. W. Stability and growth of silicalite seeds: an observation of initial breeding. *Zeolites* **1989**, *9* (6), 526−530.
(47) Warzywoda, J.; Edelman, R. D.; Thompson, R. W. Crystallization of high-silica ZSM-5 in the presence of seeds. *Zeolites* **1991**, *11* (4), 318−324.
(48) Kasahara, S.; Itabashi, K.; Igawa, K. Clear aqueous nuclei solution for faujasite synthesis. In *Studies in Surface Science and Catalysis*; Elsevier: 1986; Vol. *28*, pp 185−192.
(49) Liu, Z.; Wakihara, T.; Oshima, K.; Nishioka, D.; Hotta, Y.; Elangovan, S. P.; Yanaba, Y.; Yoshikawa, T.; Chaikittisilp, W.; Matsuo, T.; Takewaki, T.; Okubo, T. Widening synthesis bottlenecks: Realization of ultrafast and continuous-flow synthesis of high-silica zeolite SSZ-13 for NOx removal. *Angew. Chem., Int. Ed.* **2015**, *127* (19), 5775−5779.
(50) Liu, Z.; Zhu, J.; Peng, C.; Wakihara, T.; Okubo, T. Continuous flow synthesis of ordered porous materials: from zeolites to metal−organic frameworks and mesoporous silica. *Reaction Chemistry & Engineering* **2019**, *4* (10), 1699−1720.
(51) Yoshioka, T.; Liu, Z.; Iyoki, K.; Chokkalingam, A.; Yonezawa, Y.; Hotta, Y.; Ohnishi, R.; Matsuo, T.; Yanaba, Y.; Ohara, K.; Takewaki, T.; Sano, T.; Okubo, T.; Wakihara, T. Ultrafast and continuous-flow synthesis of AFX zeolite via interzeolite conversion of FAU zeolite. *React. Chem. Eng.* **2021**, *6* (1), 74−81.
(52) Niu, P.; Liu, P.; Xi, H.; Lin, M.; Wang, J.; Chen, X.; Jia, L.; Wang, P.; Hou, B.; Li, D. Crystallization mechanism of pure-silica ZSM-22 in the seed-assistant system. *Cryst. Growth Des.* **2018**, *18* (11), 6591−6601.
(53) Kamimura, Y.; Chaikittisilp, W.; Itabashi, K.; Shimojima, A.; Okubo, T. Critical factors in the seed-assisted synthesis of zeolite beta and "green beta" from OSDA-free Na+−aluminosilicate gels. *Chem. - Asian J.* **2010**, *5* (10), 2182−2191.
(54) Kamimura, Y.; Itabashi, K.; Okubo, T. Seed-assisted, OSDA-free synthesis of MTW-type zeolite and "Green MTW" from sodium aluminosilicate gel systems. *Microporous Mesoporous Mater.* **2012**, *147* (1), 149−156.
(55) Maldonado, M.; Oleksiak, M. D.; Chinta, S.; Rimer, J. D. Controlling crystal polymorphism in organic-free synthesis of Na-zeolites. *J. Am. Chem. Soc.* **2013**, *135* (7), 2641−2652.
(56) Devos, J.; Shah, M. A.; Dusselier, M. On the key role of aluminium and other heteroatoms during interzeolite conversion synthesis. *RSC Adv.* **2021**, *11* (42), 26188−26210.
(57) Bruter, D.; Pavlov, V.; Ivanova, I. Interzeolite Transformations as a Method for Zeolite Catalyst Synthesis. *Pet. Chem.* **2021**, *61* (3), 251−275.
(58) Cundy, C. S.; Cox, P. A. The hydrothermal synthesis of zeolites: Precursors, intermediates and reaction mechanism. *Microporous Mesoporous Mater.* **2005**, *82* (1−2), 1−78.
(59) Cundy, C. S.; Cox, P. A. The hydrothermal synthesis of zeolites: history and development from the earliest days to the present time. *Chem. Rev.* **2003**, *103* (3), 663−702.
(60) Subotić, B.; Bronić, J.; Jelić, T. A. Theoretical and Practical Aspects of Zeolite Nucleation. In *Ordered Porous Solids*; Elsevier: 2009; pp 127−185.
(61) Grand, J.; Awala, H.; Mintova, S. Mechanism of zeolites crystal growth: new findings and open questions. *CrystEngComm* **2016**, *18* (5), 650−664.
(62) Li, Y.; Yu, J. Emerging applications of zeolites in catalysis, separation and host−guest assembly. *Nature Reviews Materials* **2021**, *6*, 1156−1174.
(63) Mendoza-Castro, M. J.; Serrano, E.; Linares, N.; García-Martínez, J. Surfactant-templated zeolites: From thermodynamics to direct observation. *Adv. Mater. Interfaces* **2021**, *8* (4), 2001388.
(64) Itabashi, K.; Kamimura, Y.; Iyoki, K.; Shimojima, A.; Okubo, T. A working hypothesis for broadening framework types of zeolites in seed-assisted synthesis without organic structure-directing agent. *J. Am. Chem. Soc.* **2012**, *134* (28), 11542−11549.

https://doi.org/10.1021/jacs.1c11014
J. Am. Chem. Soc. 2021, 143, 21446−21460

(65) Jon, H.; Ikawa, N.; Oumi, Y.; Sano, T. An insight into the process involved in hydrothermal conversion of FAU to *BEA zeolite. *Chem. Mater.* **2008**, *20* (12), 4135−4141.
(66) Honda, K.; Itakura, M.; Matsuura, Y.; Onda, A.; Ide, Y.; Sadakane, M.; Sano, T. Role of structural similarity between starting zeolite and product zeolite in the interzeolite conversion process. *J. Nanosci. Nanotechnol.* **2013**, *13* (4), 3020−3026.
(67) Suhendar, D.; Mukti, R. R. In *Simple Approach in Understanding Interzeolite Transformations Using Ring Building Units*, The 12th Joint Conference on Chemistry Indonesia, 2018; IOP Publishing: Indonesia, 2017; p 012016.
(68) Inagaki, S.; Tsuboi, Y.; Nishita, Y.; Syahylah, T.; Wakihara, T.; Kubota, Y. Rapid synthesis of an aluminum-rich MSE-type zeolite by the hydrothermal conversion of an FAU-type zeolite. *Chem. - Eur. J.* **2013**, *19* (24), 7780−7786.
(69) Zhang, J.; Chu, Y.; Deng, F.; Feng, Z.; Meng, X.; Xiao, F.-S. Evolution of D6R units in the interzeolite transformation from FAU, MFI or *BEA into AEI: transfer or reassembly? *Inorg. Chem. Front.* **2020**, *7* (11), 2204−2211.
(70) Swaddle, T. W. Silicate complexes of aluminum (III) in aqueous systems. *Coord. Chem. Rev.* **2001**, *219*, 665−686.
(71) Mlekodaj, K.; Bernauer, M.; Olszowka, J. E.; Klein, P.; Pashkova, V.; Dedecek, J. Synthesis of the Zeolites from SBU: An SSZ-13 Study. *Chem. Mater.* **2021**, *33* (5), 1781−1788.
(72) Tanigawa, T.; Tsunoji, N.; Sadakane, M.; Sano, T. High-quality synthesis of a nanosized CHA zeolite by a combination of a starting FAU zeolite and aluminum sources. *Dalton Transactions* **2020**, *49* (29), 9972−9982.
(73) Møller, K. H.; Debost, M.; Lakiss, L.; Kegnæs, S.; Mintova, S. Interzeolite conversion of a micronsized FAU to a nanosized CHA zeolite free of organic structure directing agent with a high CO_2 capacity. *RSC Adv.* **2020**, *10* (70), 42953−42959.
(74) Goel, S.; Zones, S. I.; Iglesia, E. Encapsulation of metal clusters within MFI via interzeolite transformations and direct hydrothermal syntheses and catalytic consequences of their confinement. *J. Am. Chem. Soc.* **2014**, *136* (43), 15280−15290.
(75) Goel, S.; Wu, Z.; Zones, S. I.; Iglesia, E. Synthesis and catalytic properties of metal clusters encapsulated within small-pore (SOD, GIS, ANA) zeolites. *J. Am. Chem. Soc.* **2012**, *134* (42), 17688−17695.
(76) Limlamthong, M.; Tesana, S.; Yip, A. C. Metal encapsulation in zeolite particles: a rational design of zeolite-supported catalyst with maximum site activity. *Adv. Powder Technol.* **2020**, *31* (3), 1274−1279.
(77) Zhu, Z.; Xu, H.; Jiang, J.; Guan, Y.; Wu, P. Sn-Beta zeolite hydrothermally synthesized via interzeolite transformation as efficient Lewis acid catalyst. *J. Catal.* **2017**, *352*, 1−12.
(78) Zhang, J.; Wang, L.; Zhang, B.; Zhao, H.; Kolb, U.; Zhu, Y.; Liu, L.; Han, Y.; Wang, G.; Wang, C.; Su, D. S.; Gates, B. C.; Xiao, F.-S. Sinter-resistant metal nanoparticle catalysts achieved by immobilization within zeolite crystals via seed-directed growth. *Nat. Catal.* **2018**, *1* (7), 540−546.
(79) Wang, H.; Wang, L.; Xiao, F.-S. Metal@Zeolite hybrid materials for catalysis. *ACS Cent. Sci.* **2020**, *6* (10), 1685−1697.
(80) Ghorbanpour, A.; Gumidyala, A.; Grabow, L. C.; Crossley, S. P.; Rimer, J. D. Epitaxial growth of ZSM-5@Silicalite-1: A core−shell zeolite designed with passivated surface acidity. *ACS Nano* **2015**, *9* (4), 4006−4016.
(81) Jeon, M. Y.; Kim, D.; Kumar, P.; Lee, P. S.; Rangnekar, N.; Bai, P.; Shete, M.; Elyassi, B.; Lee, H. S.; Narasimharao, K.; et al. Ultra-selective high-flux membranes from directly synthesized zeolite nanosheets. *Nature* **2017**, *543* (7647), 690−694.
(82) Xie, B.; Zhang, H.; Yang, C.; Liu, S.; Ren, L.; Zhang, L.; Meng, X.; Yilmaz, B.; Müller, U.; Xiao, F.-S. Seed-directed synthesis of zeolites with enhanced performance in the absence of organic templates. *Chem. Commun.* **2011**, *47* (13), 3945−3947.
(83) Bouizi, Y.; Rouleau, L.; Valtchev, V. P. Factors controlling the formation of core−shell zeolite−zeolite composites. *Chem. Mater.* **2006**, *18* (20), 4959−4966.
(84) Masoumifard, N.; Guillet-Nicolas, R.; Kleitz, F. Synthesis of engineered zeolitic materials: from classical zeolites to hierarchical core−shell materials. *Adv. Mater.* **2018**, *30* (16), 1704439.
(85) Čižmek, A.; Komunjer, L.; Subotić, B.; Široki, M.; Rončević, S. Kinetics of zeolite dissolution: Part 3. Dissolution of synthetic mordenite in hot sodium hydroxide solutions. *Zeolites* **1992**, *12* (2), 190−196.
(86) Jain, R.; Rimer, J. D. Seed-Assisted zeolite synthesis: The impact of seeding conditions and interzeolite transformations on crystal structure and morphology. *Microporous Mesoporous Mater.* **2020**, *300*, 110174.
(87) Iyoki, K.; Itabashi, K.; Okubo, T. Progress in seed-assisted synthesis of zeolites without using organic structure-directing agents. *Microporous Mesoporous Mater.* **2014**, *189*, 22−30.
(88) Majano, G.; Darwiche, A.; Mintova, S.; Valtchev, V. Seed-induced crystallization of nanosized Na-ZSM-5 crystals. *Ind. Eng. Chem. Res.* **2009**, *48* (15), 7084−7091.
(89) Van Tendeloo, L.; Gobechiya, E.; Breynaert, E.; Martens, J. A.; Kirschhock, C. E. A. Alkaline cations directing the transformation of FAU zeolites into five different framework types. *Chem. Commun.* **2013**, *49* (100), 11737−11739.
(90) Breck, D. W. *Zeolite Molecular Sieves: Structure, Chemistry, and Use*; John Wiley & Sons: 1973.
(91) Khodabandeh, S.; Davis, M. E. Synthesis of CIT-3: a calcium aluminosilicate with the heulandite topology. *Microporous Mater.* **1997**, *9* (3−4), 149−160.
(92) Khodabandeh, S.; Lee, G.; Davis, M. E. CIT-4: The first synthetic analogue of brewsterite. *Microporous Mater.* **1997**, *11* (1−2), 87−95.
(93) Martín, N.; Moliner, M.; Corma, A. High yield synthesis of high-silica chabazite by combining the role of zeolite precursors and tetraethylammonium: SCR of NOx. *Chem. Commun.* **2015**, *51* (49), 9965−9968.
(94) Subotić, B.; Sekovanić, L. Transformation of zeolite A into hydroxysodalite: II. Growth kinetics of hydroxysodalite microcrystals. *J. Cryst. Growth* **1986**, *75* (3), 561−572.
(95) Subotić, B.; Škrtić, D.; Šmit, I.; Sekovanić, L. Transformation of zeolite A into hydroxysodalite: I. An approach to the mechanism of transformation and its experimental evaluation. *J. Cryst. Growth* **1980**, *50* (2), 498−508.
(96) Van Tendeloo, L.; Wangermez, W.; Vandekerkhove, A.; Willhammar, T.; Bals, S.; Maes, A.; Martens, J. A.; Kirschhock, C. E.; Breynaert, E. Postsynthetic high-alumina zeolite crystal engineering in organic-free hyper-alkaline media. *Chem. Mater.* **2017**, *29* (2), 629−638.
(97) Xie, D.; Lacheen, H. S. Separation of gases using GME framework type zeolites. US Patent US93,64,782, June 14, 2016.
(98) Bhadra, B. N.; Seo, P. W.; Jun, J. W.; Jeong, J. H.; Kim, T.-W.; Kim, C.-U.; Jhung, S. H. Syntheses of SSZ-39 and mordenite zeolites with N,N-dialkyl-2,6-dimethyl-piperidinium hydroxide/iodides: Phase-selective syntheses with anions. *Microporous Mesoporous Mater.* **2016**, *235*, 135−142.
(99) Davis, T. M. Method for preparing high-silica lev-type zeolites. US Patent US9,156,706, October 13, 2015.
(100) Dwyer, F. G.; Chu, P. ZSM-4 crystallization via faujasite metamorphosis. *J. Catal.* **1979**, *59* (2), 263−271.
(101) Inoue, T.; Itakura, M.; Jon, H.; Oumi, Y.; Takahashi, A.; Fujitani, T.; Sano, T. Synthesis of LEV zeolite by interzeolite conversion method and its catalytic performance in ethanol to olefins reaction. *Microporous Mesoporous Mater.* **2009**, *122* (1−3), 149−154.
(102) Itakura, M.; Inoue, T.; Takahashi, A.; Fujitani, T.; Oumi, Y.; Sano, T. Synthesis of high-silica CHA zeolite from FAU zeolite in the presence of benzyltrimethylammonium hydroxide. *Chem. Lett.* **2008**, *37* (9), 908−909.
(103) Itakura, M.; Ota, K.; Shibata, S.; Inoue, T.; Ide, Y.; Sadakane, M.; Sano, T. Influence of starting zeolite on synthesis of RUT type zeolite by interzeolite conversion method. *J. Cryst. Growth* **2011**, *314* (1), 274−278.

https://doi.org/10.1021/jacs.1c11014
J. Am. Chem. Soc. 2021, 143, 21446−21460

(104) Martín, N.; Boruntea, C. R.; Moliner, M.; Corma, A. Efficient synthesis of the Cu-SSZ-39 catalyst for DeNOx applications. *Chem. Commun.* **2015**, *51* (55), 11030−11033.
(105) Martín, N.; Paris, C.; Vennestrøm, P. N.; Thøgersen, J. R.; Moliner, M.; Corma, A. Cage-based small-pore catalysts for NH_3-SCR prepared by combining bulky organic structure directing agents with modified zeolites as reagents. *Appl. Catal., B* **2017**, *217*, 125−136.
(106) Shibata, S.; Itakura, M.; Ide, Y.; Sadakane, M.; Sano, T. FAU−LEV interzeolite conversion in fluoride media. *Microporous Mesoporous Mater.* **2011**, *138* (1−3), 32−39.
(107) Zones, S. Conversion of faujasites to high-silica chabazite SSZ-13 in the presence of N,N,N-trimethyl-1-adamantammonium iodide. *J. Chem. Soc., Faraday Trans.* **1991**, *87* (22), 3709−3716.
(108) Zones, S.; Nakagawa, Y. Use of modified zeolites as reagents influencing nucleation in zeolite synthesis. In *Studies in Surface Science and Catalysis*; Elsevier: 1995; Vol. *97*, pp 45−52.
(109) Zones, S. I.; Lew, C. M.; Xie, D.; Davis, T. M.; Schmidt, J. E.; Saxton, R. J. Studies on the use of faujasite as a reagent to deliver silica and alumina in building new zeolite structures with organo-cations. *Microporous Mesoporous Mater.* **2020**, *300*, 110162.
(110) Goel, S.; Zones, S. I.; Iglesia, E. Synthesis of zeolites via interzeolite transformations without organic structure-directing agents. *Chem. Mater.* **2015**, *27* (6), 2056−2066.
(111) Yashiki, A.; Honda, K.; Fujimoto, A.; Shibata, S.; Ide, Y.; Sadakane, M.; Sano, T. Hydrothermal conversion of FAU zeolite into LEV zeolite in the presence of non-calcined seed crystals. *J. Cryst. Growth* **2011**, *325* (1), 96−100.
(112) Qin, W.; Jain, R.; Robles Hernández, F. C.; Rimer, J. D. Organic-free interzeolite transformation in the absence of common building units. *Chem. - Eur. J.* **2019**, *25* (23), 5893−5898.
(113) dos Santos, M. B.; Vianna, K. C.; Pastore, H. O.; Andrade, H. M.; Mascarenhas, A. J. Studies on the synthesis of ZSM-5 by interzeolite transformation from zeolite Y without using organic structure directing agents. *Microporous Mesoporous Mater.* **2020**, *306*, 110413.
(114) Wang, B.; Ren, L.; Zhang, J.; Peng, R.; Jin, S.; Guan, Y.; Xu, H.; Wu, P. Ultrafast synthesis of high-silica Beta zeolite from dealuminated MOR by interzeolite transformation for methanol to propylene reactions. *Microporous Mesoporous Mater.* **2021**, *314*, 110894.
(115) Liang, Y.; Jacobson, A. J.; Rimer, J. D. Strontium ions function as both an accelerant and structure-directing agent of chabazite crystallization. *ACS Materials Letters* **2021**, *3* (2), 187−192.
(116) Kubota, Y.; Maekawa, H.; Miyata, S.; Tatsumi, T.; Sugi, Y. Hydrothermal synthesis of metallosilicate SSZ-24 from metallosilicate beta as precursors. *Microporous Mesoporous Mater.* **2007**, *101* (1−2), 115−126.
(117) Zones, S. I.; Santilli, D. S. Hydrocarbon conversion processes using zeolite SSZ-41. US Patent US5,656,149, August 12, 1997.
(118) Xie, D.; Zones, S. I.; Lew, C. M.; Davis, T. M. Molecular sieve SSZ-98. US Patent US9,409,786, August 9, 2016.
(119) Nishitoba, T.; Yoshida, N.; Kondo, J. N.; Yokoi, T. Control of Al Distribution in the CHA-Type Aluminosilicate Zeolites and Its Impact on the Hydrothermal Stability and Catalytic Properties. *Ind. Eng. Chem. Res.* **2018**, *57* (11), 3914−3922.
(120) Muraoka, K.; Sada, Y.; Shimojima, A.; Chaikittisilp, W.; Okubo, T. Tracking the rearrangement of atomic configurations during the conversion of FAU zeolite to CHA zeolite. *Chemical Science* **2019**, *10* (37), 8533−8540.
(121) Devos, J.; Bols, M. L.; Plessers, D.; Goethem, C. V.; Seo, J. W.; Hwang, S.-J.; Sels, B. F.; Dusselier, M. Synthesis−structure−activity relations in Fe-CHA for C−H activation: control of Al distribution by interzeolite conversion. *Chem. Mater.* **2020**, *32* (1), 273−285.
(122) Onishi, M.; Tsunoji, N.; Sadakane, M.; Sano, T. Synthesis of Phosphorus-Modified AFX Zeolite by the Hydrothermal Conversion of Tetraalkylphosphonium Hydroxide-Impregnated FAU Zeolite. *Bull. Chem. Soc. Jpn.* **2021**, *94* (1), 1−7.
(123) Takata, T.; Tsunoji, N.; Takamitsu, Y.; Sadakane, M.; Sano, T. Incorporation of various heterometal atoms in CHA zeolites by hydrothermal conversion of FAU zeolite and their performance for selective catalytic reduction of NOx with ammonia. *Microporous Mesoporous Mater.* **2017**, *246*, 89−101.
(124) Ma, H.; Zhu, Z.; Tang, P.; Su, T.; Wu, P.; Lü, H. Hierarchical Ti-Beta zeolites with uniform intracrystalline mesopores hydrothermally synthesized via interzeolite transformation for oxidative desulfurization. *Microporous Mesoporous Mater.* **2021**, *311*, 110702.
(125) Kunitake, Y.; Takata, T.; Yamasaki, Y.; Yamanaka, N.; Tsunoji, N.; Takamitsu, Y.; Sadakane, M.; Sano, T. Synthesis of titanated chabazite with enhanced thermal stability by hydrothermal conversion of titanated faujasite. *Microporous Mesoporous Mater.* **2015**, *215*, 58−66.
(126) Funase, N.; Takata, T.; Tsunoji, N.; Takamitsu, Y.; Sadakane, M.; Sano, T. Hydrothermal conversion of titanated FAU to AEI zeolite and Its enhanced catalytic performance for NOx reduction. *Adv. Porous Mater.* **2016**, *4* (1), 62−72.
(127) Chen, C.-T.; Iyoki, K.; Hu, P.; Yamada, H.; Ohara, K.; Sukenaga, S.; Ando, M.; Shibata, H.; Okubo, T.; Wakihara, T. Reaction Kinetics Regulated Formation of Short-Range Order in an Amorphous Matrix during Zeolite Crystallization. *J. Am. Chem. Soc.* **2021**, *143* (29), 10986−10997.
(128) Choudhary, M. K.; Jain, R.; Rimer, J. D. In situ imaging of two-dimensional surface growth reveals the prevalence and role of defects in zeolite crystallization. *Proc. Natl. Acad. Sci. U. S. A.* **2020**, *117* (46), 28632−28639.
(129) Hamilton, K. E.; Coker, E. N.; Sacco, A., Jr.; Dixon, A. G.; Thompson, R. W. The effects of the silica source on the crystallization of zeolite NaX. *Zeolites* **1993**, *13* (8), 645−653.
(130) Krznarić, I.; Antonić, T.; Bronić, J.; Subotić, B.; Thompson, R. W. Influence of silica sources on the chemical composition of aluminosilicate hydrogels and the results of their hydrothermal treatment. *Croat. Chem. Acta* **2003**, *76* (1), 7−17.
(131) Ostwald, W. Studien über die bildung und umwandlung fester körper. *Z. Phys. Chem.* **1897**, *22* (1), 289−330.
(132) Shen, Y.; Le, T. T.; Li, R.; Rimer, J. D. Optimized synthesis of ZSM-11 catalysts using 1,8-diaminooctane as a structure-directing agent. *ChemPhysChem* **2018**, *19* (4), 529−537.
(133) Hincapie, B. O.; Garces, L. J.; Zhang, Q.; Sacco, A.; Suib, S. L. Synthesis of mordenite nanocrystals. *Microporous Mesoporous Mater.* **2004**, *67* (1), 19−26.
(134) Yue, M. B.; Yang, N.; Jiao, W. Q.; Wang, Y. M.; He, M.-Y. Dry-gel synthesis of shaped binderless zeolites composed of nanosized ZSM-5. *Solid State Sci.* **2013**, *20*, 1−7.
(135) Rimer, J. D.; Kumar, M.; Li, R.; Lupulescu, A. I.; Oleksiak, M. D. Tailoring the physicochemical properties of zeolite catalysts. *Catal. Sci. Technol.* **2014**, *4* (11), 3762−3771.
(136) Goto, I.; Itakura, M.; Shibata, S.; Honda, K.; Ide, Y.; Sadakane, M.; Sano, T. Transformation of LEV-type zeolite into less dense CHA-type zeolite. *Microporous Mesoporous Mater.* **2012**, *158*, 117−122.
(137) Honda, K.; Yashiki, A.; Itakura, M.; Ide, Y.; Sadakane, M.; Sano, T. Influence of seeding on FAU−*BEA interzeolite conversions. *Microporous Mesoporous Mater.* **2011**, *142* (1), 161−167.
(138) Sogukkanli, S.; Iyoki, K.; Elangovan, S. P.; Itabashi, K.; Takano, M.; Liu, Z.; Inagaki, S.; Wakihara, T.; Kubota, Y.; Okubo, T. Rational seed-directed synthesis of MSE-type zeolites using a simple organic structure-directing agent by extending the composite building unit hypothesis. *Microporous Mesoporous Mater.* **2017**, *245*, 1−7.
(139) Muraoka, K.; Sada, Y.; Miyazaki, D.; Chaikittisilp, W.; Okubo, T. Linking synthesis and structure descriptors from a large collection of synthetic records of zeolite materials. *Nat. Commun.* **2019**, *10* (1), 1−11.
(140) Schwalbe-Koda, D.; Jensen, Z.; Olivetti, E.; Gómez-Bombarelli, R. Graph similarity drives zeolite diffusionless transformations and intergrowth. *Nat. Mater.* **2019**, *18* (11), 1177−1181.
(141) Navrotsky, A.; Trofymluk, O.; Levchenko, A. A. Thermochemistry of microporous and mesoporous materials. *Chem. Rev.* **2009**, *109* (9), 3885−3902.

(142) Petrovic, I.; Navrotsky, A. Thermochemistry of Na-faujasites with varying Si/Al ratios. *Microporous Mater.* **1997**, *9* (1−2), 1−12.
(143) Golov, A. A.; Blatova, O. A.; Blatov, V. A. Perceiving zeolite self-assembly: A combined top-down and bottom-up approach within the tiling model. *J. Phys. Chem. C* **2020**, *124* (2), 1523−1528.
(144) Li, R.; Linares, N.; Sutjianto, J. G.; Chawla, A.; Garcia-Martinez, J.; Rimer, J. D. Ultrasmall zeolite L crystals prepared from highly interdispersed alkali-silicate precursors. *Angew. Chem., Int. Ed.* **2018**, *57* (35), 11283−11288.
(145) Awala, H.; Gilson, J.-P.; Retoux, R.; Boullay, P.; Goupil, J.-M.; Valtchev, V.; Mintova, S. Template-free nanosized faujasite-type zeolites. *Nat. Mater.* **2015**, *14* (4), 447−451.
(146) Choi, M.; Na, K.; Kim, J.; Sakamoto, Y.; Terasaki, O.; Ryoo, R. Stable single-unit-cell nanosheets of zeolite MFI as active and long-lived catalysts. *Nature* **2009**, *461* (7261), 246−249.
(147) Zhang, X.; Liu, D.; Xu, D.; Asahina, S.; Cychosz, K. A.; Agrawal, K. V.; Al Wahedi, Y.; Bhan, A.; Al Hashimi, S.; Terasaki, O.; Thommes, M.; Tsapatsis, M. Synthesis of self-pillared zeolite nanosheets by repetitive branching. *Science* **2012**, *336* (6089), 1684−1687.
(148) Schwalbe-Koda, D.; Kwon, S.; Paris, C.; Bello-Jurado, E.; Jensen, Z.; Olivetti, E.; Willhammar, T.; Corma, A.; Roman-Leshkov, Y.; Moliner, M.; Gómez-Bombarelli, R. A priori control of zeolite phase competition and intergrowth with high-throughput simulations. *Science* **2021**, *374*, 308−315.
(149) Luo, H. Y.; Michaelis, V. K.; Hodges, S.; Griffin, R. G.; Román-Leshkov, Y. One-pot synthesis of MWW zeolite nanosheets using a rationally designed organic structure-directing agent. *Chemical Science* **2015**, *6* (11), 6320−6324.
(150) Kim, J.; Jo, C.; Lee, S.; Ryoo, R. Bulk crystal seeding in the generation of mesopores by organosilane surfactants in zeolite synthesis. *J. Mater. Chem. A* **2014**, *2* (30), 11905−11912.
(151) Moliner, M.; Román-Leshkov, Y.; Corma, A. Machine learning applied to zeolite synthesis: the missing link for realizing high-throughput discovery. *Acc. Chem. Res.* **2019**, *52* (10), 2971−2980.
(152) Jensen, Z.; Kwon, S.; Schwalbe-Koda, D.; Paris, C.; Gómez-Bombarelli, R.; Román-Leshkov, Y.; Corma, A.; Moliner, M.; Olivetti, E. A. Discovering relationships between OSDAs and zeolites through data mining and generative neural networks. *ACS Cent. Sci.* **2021**, *7* (5), 858−867.
(153) Yang, S.; Lach-hab, M.; Vaisman, I. I.; Blaisten-Barojas, E. Identifying zeolite frameworks with a machine learning approach. *J. Phys. Chem. C* **2009**, *113* (52), 21721−21725.
(154) Moliner, M.; Serra, J.; Corma, A.; Argente, E.; Valero, S.; Botti, V. Application of artificial neural networks to high-throughput synthesis of zeolites. *Microporous Mesoporous Mater.* **2005**, *78* (1), 73−81.
(155) Valtchev, V.; Tosheva, L. Porous nanosized particles: preparation, properties, and applications. *Chem. Rev.* **2013**, *113* (8), 6734−6760.
(156) Eliášová, P.; Opanasenko, M.; Wheatley, P. S.; Shamzhy, M.; Mazur, M.; Nachtigall, P.; Roth, W. J.; Morris, R. E.; Čejka, J. The ADOR mechanism for the synthesis of new zeolites. *Chem. Soc. Rev.* **2015**, *44* (20), 7177−7206.
(157) Opanasenko, M.; Shamzhy, M.; Wang, Y.; Yan, W.; Nachtigall, P.; Čejka, J. Synthesis and Post-Synthesis Transformation of Germanosilicate Zeolites. *Angew. Chem., Int. Ed.* **2020**, *59* (44), 19380−19389.
(158) Flanigen, E. M.; Patton, R. L. Silica polymorph and process for preparing same. US Patent US4,073,865, February 14, 1978.
(159) Kumar, M.; Luo, H.; Román-Leshkov, Y.; Rimer, J. D. SSZ-13 crystallization by particle attachment and deterministic pathways to crystal size control. *J. Am. Chem. Soc.* **2015**, *137* (40), 13007−13017.
(160) Vega-Vila, J. C.; Gounder, R. Quantification of Intraporous Hydrophilic Binding Sites in Lewis Acid Zeolites and Consequences for Sugar Isomerization Catalysis. *ACS Catal.* **2020**, *10* (20), 12197−12211.
(161) Guth, J. L.; Kessler, H.; Higel, J. M.; Lamblin, J. M.; Patarin, J.; Seive, A.; Chezeau, J. M.; Wey, R. Zeolite Synthesis in the Presence of Fluoride Ions. In *Zeolite Synthesis*; American Chemical Society: 1989; Vol. *398*, pp 176−195.
(162) Aykol, M.; Hegde, V. I.; Hung, L.; Suram, S.; Herring, P.; Wolverton, C.; Hummelshøj, J. S. Network analysis of synthesizable materials discovery. *Nat. Commun.* **2019**, *10* (1), 1−7.
(163) Yamada, H.; Liu, C.; Wu, S.; Koyama, Y.; Ju, S.; Shiomi, J.; Morikawa, J.; Yoshida, R. Predicting materials properties with little data using shotgun transfer learning. *ACS Cent. Sci.* **2019**, *5* (10), 1717−1730.
(164) Datar, A.; Chung, Y. G.; Lin, L.-C. Beyond the BET analysis: the surface area prediction of nanoporous materials using a machine learning method. *J. Phys. Chem. Lett.* **2020**, *11* (14), 5412−5417.
(165) Tanaka, K.; Hachiya, K.; Zhang, W.; Matsuda, K.; Miyauchi, Y. Machine-learning analysis to predict the exciton valley polarization landscape of 2D semiconductors. *ACS Nano* **2019**, *13* (11), 12687−12693.
(166) Tao, H.; Wu, T.; Aldeghi, M.; Wu, T. C.; Aspuru-Guzik, A.; Kumacheva, E. Nanoparticle synthesis assisted by machine learning. *Nat. Rev. Mater.* **2021**, *6*, 701−716.

https://doi.org/10.1021/jacs.1c11014
J. Am. Chem. Soc. 2021, 143, 21446−21460